

Growing the first bright quasars in cosmological simulations of structure formation

Debora Sijacki^{1*}, Volker Springel² and Martin G. Haehnelt¹

¹ *Kavli Institute for Cosmology, Cambridge and Institute of Astronomy, Madingley Road, Cambridge, CB3 0HA*

² *Max-Planck-Institut für Astrophysik, Karl-Schwarzschild-Straße 1, 85740 Garching bei München, Germany*

30 October 2018

ABSTRACT

We employ cosmological hydrodynamical simulations to study the growth of massive black holes (BHs) at high redshifts subject to BH merger recoils from gravitational wave emission. As a promising host system of a powerful high-redshift quasar, we select the most massive dark matter halo at $z = 6$ from the Millennium simulation, and resimulate its formation at much higher resolution including gas physics and a model for BH seeding, growth and feedback. Assuming that the initial BH seeds are relatively massive, of the order of $10^5 M_{\odot}$, and that seeding occurs around $z \sim 15$ in dark matter haloes of mass $\sim 10^9 - 10^{10} M_{\odot}$, we find that it is possible to build up supermassive BHs (SMBHs) by $z = 6$ that assemble most of their mass during extended Eddington-limited accretion periods. The properties of the simulated SMBHs are consistent with observations of $z = 6$ quasars in terms of the estimated BH masses and bolometric luminosities, the amount of star formation occurring within the host halo, and the presence of highly enriched gas in the innermost regions of the host galaxy. After a peak in the BH accretion rate at $z = 6$, the most massive BH has become sufficiently massive for the growth to enter into a much slower phase of feedback-regulated accretion. We extend our basic BH model by incorporating prescriptions for the BH recoils caused by gravitational wave emission during BH merger events, taking into account the newest numerical relativity simulations of merging BH binaries. In order to explore the full range of expected recoils and radiative efficiencies we also consider models with spinning BHs. In the most ‘pessimistic’ case where BH spins are initially high, we find that the growth of the SMBHs can be potentially hampered if they grow mostly in isolation and experience only a small number of mergers. On the other hand, whereas BH kicks can expel a substantial fraction of low mass BHs, they do not significantly affect the build up of the SMBHs. On the contrary, a large number of BH mergers has beneficial consequences for the growth of the SMBHs by considerably reducing their spin. We also track the fate of our $z = 6$ SMBH by performing cosmological simulations all the way to $z = 2$. This allows us to study the history of BH mass assembly over a large time-span and to establish a clear signal of ‘downsizing’ of the BH accretion rate for the population of BHs as a whole. We further find that the descendants of the most luminous $z = 6$ quasar correspond most likely to the most massive BHs today, characterized by a low activity level and masses of the order of $1 - 2 \times 10^{10} M_{\odot}$.

Key words: methods: numerical – black hole physics – cosmology: theory

1 INTRODUCTION

Black holes (BHs) are among the most remarkable objects in the Universe. They are now widely believed to power quasars (Schmidt, 1963; Salpeter, 1964; Lynden-Bell, 1969), which

belong to the most luminous sources we know of. Furthermore, BHs are associated with the relativistic acceleration of particles, jet formation, and the presence of radio lobes (Begelman et al., 1984; Rees, 1984), which are often accompanied by copious outflows and shocks. Given that solid observational evidence (Dressler, 1989; Kormendy & Richstone, 1995; Magorrian et al., 1998) indicates that BHs are

* E-mail: deboras@ast.cam.ac.uk

ubiquitous inhabitants of a vast majority of galaxies and that their properties correlate with those of their host systems, it is inevitable to conclude that BHs should in some way influence their host galaxies, and that in turn BHs could depend on the properties of the galaxies they live in.

A number of well defined relationships between the BH mass and the central stellar properties of the host galaxy, like its bulge velocity dispersion, mass, and luminosity have been recently established (e.g. Ferrarese & Merritt, 2000; Gebhardt et al., 2000; Tremaine et al., 2002; Magorrian et al., 1998; Marconi & Hunt, 2003; Häring & Rix, 2004). These observational findings have prompted a large body of theoretical research (Ciotti & Ostriker, 1997; Silk & Rees, 1998; Haehnelt et al., 1998; Fabian & Iwasawa, 1999; Kauffmann & Haehnelt, 2000; King, 2003; Wyithe & Loeb, 2003; Di Matteo et al., 2005; Hopkins et al., 2006; Croton et al., 2006; Bower et al., 2006; Okamoto et al., 2008), which focused on understanding how BHs and galaxies coevolve. It appears clear that any successful model of cosmic structure formation needs to incorporate BHs and their feedback effects, but it is still far less clear which mechanisms are ultimately responsible for BH feeding and feedback. The difficulty lies in the inherent complexity of the problem, where a vast range of scales and an array of non-linear physical processes need to be considered.

It is beyond the current capabilities of any numerical code to self-consistently follow the relevant gravitational, magneto-hydrodynamical, and star formation processes over the full dynamic range necessary for an ab-initio treatment, from the size of the BH's sphere of influence all the way up to cosmologically representative scales. Nonetheless, in the last few years rapid progress has been made on three different fronts regarding direct numerical simulations of BHs. At the smallest scales, full general relativity simulations of BH binary mergers have become recently possible (e.g. Pretorius, 2007; Campanelli et al., 2007; Herrmann et al., 2007; Koppitz et al., 2007; González et al., 2007; Baker et al., 2008). This has greatly improved our understanding of the interaction of BHs in these extreme situations, and of the consequences these interactions have on much larger scales. The second breakthrough has been accomplished in full general relativity magnetohydrodynamic simulations of BH accretion disks (Koide et al., 1999; Gammie et al., 2003; De Villiers & Hawley, 2003; McKinney & Gammie, 2004; Hawley & Krolik, 2006; Beckwith et al., 2008). In these studies it has been convincingly demonstrated that BH accretion processes are indeed able of producing relativistic jets and outflows, which also should have an impact on much larger scales. Finally, on cosmological scales it has become possible, for the first time, to simulate the evolution of BHs embedded in a range of host haloes and to follow their growth and feedback over cosmic time simultaneously with the build-up of their host galaxies and the surrounding cosmic large-scale structure (Springel et al., 2005b; Sijacki et al., 2007; Di Matteo et al., 2008). However, a crucial aspect that is currently still missing is a connection between these different simulation techniques, which would give us a much more complete and compelling picture.

One approach to overcome the present numerical limitations is to construct sub-resolution models which encapsulate physical processes occurring on the scales below the achievable spatial resolution of the simulation, and then

to test these sub-resolution prescriptions in full cosmological simulations against the available observational findings. This is the approach that we have taken already in Sijacki et al. (2007, 2008), where we have validated our BH model in cosmological simulations of BH-heated galaxies and galaxy clusters, and in simulations of cosmic ray heating in clusters due to central BH activity.

However, one of the important issues that we have not addressed in full yet is the formation of BHs at very high redshifts, in particular in the light of the existence of supermassive BHs (SMBHs) as early as $z \sim 6$, as observations of the most distant quasars in the Sloan Digital Sky Survey (SDSS) seem to indicate (Fan et al., 2001, 2003, 2004, 2006). This is exactly the problem we want to address here. The formation of SMBHs with masses of the order of $10^9 M_\odot$ in less than a Gyr of cosmic time proves to be a significant challenge for theoretical models despite their rareness and thus their very low space density (Fan, 2006). The estimated bolometric luminosities, accretion rates and masses of more than a dozen known SDSS quasars at $z \sim 6$ indicate that these objects have extreme properties, accreting at a rate very close to the Eddington rate with bolometric luminosities between 10^{47} and $10^{48} \text{ erg s}^{-1}$ (Willott et al., 2003; Barth et al., 2003; Jiang et al., 2006; Kurk et al., 2007; Fan, 2006).

Thus, the SDSS quasars represent important benchmarks for theoretical models of BH formation and growth. Several semi-analytical and hybrid numerical approaches have been employed to study the formation of BHs at high redshifts (Wyithe & Loeb, 2003; Bromm & Loeb, 2003; Volonteri et al., 2003; Volonteri & Rees, 2005, 2006; Pelupessy et al., 2007; Li et al., 2007), exploring various pathways that could lead to the formation of sufficiently massive BHs at $z = 6$. Li et al. (2007), in particular, used hydrodynamical simulations of multiple mergers of gas-rich disk galaxies to study the formation of SMBHs at high redshift. Here we will take a different approach and simulate the formation of SMBHs at $z = 6$ for the first time in fully self-consistent cosmological simulations of structure formation. We select the most massive halo from the Millennium simulation at this epoch as a promising possible host of a bright high- z quasar, and we resimulate its formation with much higher mass and spatial resolution, adopting the BH simulation model of Springel et al. (2005b) and Sijacki et al. (2007). In previous work we have shown that this BH model can successfully reproduce the observed low-redshift BH mass density, the relationships between BHs and their host galaxies, and the absence of an overcooling problem in clusters. Here we want to investigate the important question whether the same model is also capable of producing SMBHs at very high redshift.

Our second aim is to extend our default BH model by exploring different physical mechanisms which could potentially hamper the formation of massive BHs at early times. With the advent of numerical relativity simulations of binary BH mergers, it is now possible to explore the significant consequences of gravitational recoils for the build up of the whole population of BHs. Depending on the mass ratio of the merging BHs, and on the magnitudes and orientations of their spins, the remnant BH can even be expelled entirely from its host halo. Such ejections could happen more frequently at high redshifts, where the potential wells of the

BH host systems are expected to be shallower. In addition, a merger of two non-spinning BHs produces in general a spinning BH. It appears likely that theoretical models which ignore BH spins may miss an important aspect of the problem. We therefore take advantage of the newest numerical relativity results and incorporate prescriptions for BH recoils caused by asymmetric gravitational wave emission during a BH merger, where BHs are characterized by a non-vanishing spin value. We also allow for spin-dependent radiative efficiencies for gas accretion. First attempts in this direction have recently been made by Berti & Volonteri (2008) and Tanaka & Haiman (2008) using semi-analytical techniques. In this study, we employ fully cosmological hydrodynamic simulations, which provide detailed information about the merging histories of the host haloes and their central BHs, about the thermodynamic properties of the gas in the vicinity of BHs, and thus about the BH accretion and feedback processes.

Finally, we also examine the fate of the most massive high redshift BHs at lower redshifts. For this purpose we select descendents of our $z = 6$ halo at $z = 4$ and $z = 2$, and resimulate them once more adopting the same BH model and numerical resolution. This permits us to track BH activity over a much larger time span and to relate it to the dynamical history of the host halo.

The paper is organised as follows. In Section 2, we discuss the methodology we have adopted to simulate the high redshift evolution of BHs, while in Section 3 we describe the suite of simulations we have performed. The bulk of our results are presented in Sections 4 and 5, and in Section 6, we discuss our main findings and draw our conclusions.

2 METHODOLOGY

2.1 The numerical code

In this study we use the massively parallel Tree-SPH code GADGET-3 (see Springel, 2005, for a description of an earlier version of the code) in its entropy conserving formulation (Springel & Hernquist, 2002). In addition to gravity and non-radiative hydrodynamics of the dark matter and gas components, the code follows radiative cooling and heating of an optically thin plasma of hydrogen and helium, subject to a time-dependent and spatially uniform UV background. We adopt a subresolution multi-phase model for the treatment of star formation and the associated supernovae feedback, as described in Springel & Hernquist (2003), and include an optional extension for starburst powered galactic winds of constant outflow speed. We follow self-consistently the growth and feedback processes of a population of BHs embedded in the simulations. In Section 2.2, we briefly summarize the main features of our default BH model (for a more detailed description see Di Matteo et al., 2005; Springel et al., 2005b; Sijacki et al., 2007). We then discuss in more depth several extensions of the default BH model in order to account for recoils due to BH mergers induced by asymmetric gravitational wave emission. We also study models with spinning BHs and explore the evolution of the spin history in simple terms. This allows us to account for the effect of spin-dependent radiative efficiencies.

2.2 Default BH model

BHs are represented by collisionless sink particles in the code that can grow with time from an initially small mass by accreting surrounding gaseous material, or by merging with other BHs. Note that due to inevitable numerical limitations we cannot track nor resolve the initial formation processes of BHs. We assume these to be sufficiently efficient to generate a population of BH *seeds* at high redshifts in all haloes above a given mass threshold. Once such seed BH particles exist, we can then follow their subsequent growth in mass by gas accretion. The accretion rate is parametrized in terms of a simple spherically symmetric Bondi-Hoyle type accretion flow (Hoyle & Lyttleton, 1939; Bondi & Hoyle, 1944; Bondi, 1952), i.e.

$$\dot{M}_{\text{BH}} = \frac{4\pi\alpha G^2 M_{\text{BH}}^2 \rho}{(c_s^2 + v^2)^{3/2}}, \quad (1)$$

where α is a dimensionless parameter, ρ is the density, c_s the sound speed of the gas, and v is the velocity of the BH relative to the gas. Here we fix the value of α to 100, as it has been done in all of our previous work (Sijacki et al., 2007, 2008; Puchwein et al., 2008). Note that a value of α larger than unity has been adopted because cosmological simulations typically fail to resolve the Bondi radius, and thus underpredict the gas density used in equation (1). Furthermore, at the highest resolved densities we model the gas with a sub-resolution multiphase model for star formation that gives a comparatively high mean gas temperature as a result of supernova feedback. A volume-average of the Bondi-rates for the (spatially unresolved) cold and hot phases of the ISM recovers a value of α close to 100. Our results, however, are not very sensitive to the adopted value for the α parameter because most of the BH growth occurs during phases of Eddington limited accretion (where the accretion rate is independent of α), and because BH growth is self-regulated by feedback (see also Section 4.1). We furthermore assume that the accretion rate cannot exceed the Eddington limit.

BHs are also allowed to grow in mass by merging with other BHs that happen to be in the immediate vicinity (within the smoothing lengths that is used to estimate the local gas density) and that have small relative velocities of the order of or lower than the local gas sound speed. Note that our cosmological simulations lack the spatial resolution to track the BH binary hardening process at parsec and sub-parsec scales prior to the merging event (see e.g. Begelman et al., 1980). Our prescription for BH merging assumes instead that the hardening is efficient and occurs on a short timescale. This should justify that two BHs merge instantaneously when they are sufficiently close as in our model. We note that whether or not a BH binary may get ‘hung up’ for a significant time if the hardening only has to rely on stellar dynamics is still not completely settled. However, in the gas rich environments (see e.g. Escala et al., 2004; Cuadra et al., 2009) that we are discussing here, additional dissipation due to the gas should help. The procedure we have adopted should thus result in an upper bound for the possible impact of BH recoils on the growth of early quasars.

In our model, accreting BHs affect their environment by an isotropic coupling of a small fraction of their bolometric luminosity to the thermal energy of the surrounding gas particles according to the expression

$$\dot{E}_{\text{feed}} = \epsilon_f L_r = \epsilon_f \epsilon_r \dot{M}_{\text{BH}} c^2. \quad (2)$$

Here ϵ_r is the radiative efficiency which in the default model is fixed to be 0.1, while for the thermal coupling efficiency, ϵ_f , a value of 5% has been adopted. With this choice of ϵ_f , the simulated $M_{\text{BH}} - \sigma_*$ relation obtained for remnants of isolated galaxy mergers is in a good agreement with observations, as shown by Di Matteo et al. (2005). Moreover, it has been demonstrated that in fully self-consistent cosmological simulations the $M_{\text{BH}} - \sigma_*$ relation is also reproduced with this feedback efficiency (Sijacki et al., 2007; Di Matteo et al., 2008).

2.3 Choice of BH seed mass and seeding procedure

Two important issues in studying the build-up of a population of massive BHs at high redshifts are the assumed BH seed mass and the selection of haloes which contain such seeds. Both of these issues are intimately linked to poorly understood BH formation processes in the early Universe. In fact, there are several possible channels of BH formation (Rees, 1978) at early times. In this work, we are mainly interested in scenarios where relatively massive BH seeds are produced as a consequence of central gas collapse within protogalactic haloes (e.g. Haehnelt & Rees, 1993; Umemura et al., 1993; Begelman et al., 2006; Lodato & Natarajan, 2006). In this picture, the most favourable conditions for the formation of massive BH seeds with mass of order $10^4 - 10^6 h^{-1} M_\odot$ occur in haloes with virial temperatures of 10^4 K and above, and where metal line and H_2 cooling is subdominant with respect to atomic hydrogen cooling, thus preventing excessive fragmentation and star formation (Bromm & Loeb, 2003). Recently, there have been several promising numerical attempts targeted to address this specific BH formation scenario (Wise et al., 2008; Levine et al., 2008; Regan & Haehnelt, 2009), suggesting that this mechanism may indeed work.

We mimic such a scenario of BH seed formation, by assuming that the BH particles in the code are initially characterised by a fixed mass of $10^5 h^{-1} M_\odot$, and that all haloes above a given mass threshold contain at least one such BH seed. We have, however, run an additional simulation with a larger seed mass of $10^6 h^{-1} M_\odot$, in order to test the sensitivity to this choice (see Section 4.6). As in Sijacki et al. (2007), the actual creation of BH seeds in the simulations is accomplished on the fly by frequently invoking a fast and parallel friends-of-friends algorithm for halo finding; if a halo above the mass threshold is found that does not contain any BH yet, a seed BH at the halo centre is introduced. For the halo threshold value we explore two possibilities, one where the threshold value corresponds to $10^9 h^{-1} M_\odot$, and another, more restrictive case where only haloes with mass above $10^{10} h^{-1} M_\odot$ are seeded. Our main aim here is to understand whether and under which conditions such a population of BH seeds produced at high redshifts will evolve into BHs as massive as those discovered at $z = 6$. Clearly, it is also important to understand if much smaller BH seeds – possibly the remnants of the first Pop-III stars – or BH seeds populating different haloes may also give rise to the formation of luminous SDSS quasars. We defer an investi-

gation of this question, which is beyond the scope of this study, to forthcoming work.

2.4 Recoils of merging BHs

One of the potential hazards for early BH assembly are the recoils of the remnant BH due to gravitational wave emission during binary BH mergers. For certain BH binary configurations, these recoils are characterised by relatively large kick velocities which can expel a remnant BH from its host halo, especially at high redshifts where the host haloes typically have shallow potential wells (e.g. Merritt et al., 2004; Haiman, 2004; Volonteri & Rees, 2006).

Over the past two to three years, there has been a remarkable breakthrough in numerical simulations of BH binaries in full general relativity (for a recent review, see Pretorius, 2007). These simulations provide for the first time reliable estimates of the remnant BH kick velocities for various initial configurations. The full parameter space of encounters of two BHs has not been explored yet, and merger simulations involving multiple BHs are still in their infancy (see Campanelli et al., 2008). However, the results of the present day numerical relativity BH merger calculations can already be applied to cosmological simulations of BH growth in different interesting cases. In this study, we focus on the following three scenarios^{*}:

2.4.1 Mass asymmetry driven BH recoils

In our first case we consider the recoil of a BH merger remnant that is caused only by the mass difference of two non-spinning progenitor BHs. The kick velocity can then be expressed by the standard Fitchett formula (Fitchett, 1983) that has now been calibrated by numerical relativity simulations (González et al., 2007),

$$v_{\text{m, kick}} = A\eta^2 \sqrt{1 - 4\eta} (1 + B\eta). \quad (3)$$

The coefficients A and B are 1.2×10^4 and -0.93 , respectively, and $\eta = q/(1+q)^2$ is a function of the mass ratio of the progenitors only, with $q = m_1/m_2 \leq 1$. Here the maximum kick velocity is relatively low, of order 175 km s^{-1} , and occurs in the case of a mass ratio of ~ 0.36 . Note that even though the progenitor BHs are non-spinning, the remnant BH will have non-vanishing spin due to the angular momentum carried away by the gravitational wave emission. The final spin of the remnant BH can be expressed as a function of the η parameter only, i.e. $a_{\text{fin}} = 3.464\eta - 2.029\eta^2$ (Berti et al., 2007).

2.4.2 Recoils in configurations with arbitrary mass ratio and aligned/anti-aligned spins

In the next case we explore encounters of two BHs with arbitrary mass ratio and non-vanishing spins[†]. However, we impose that the two BH spins prior to the merger are either aligned or anti-aligned with the orbital angular momentum vector, with equal probability. The absolute values of the

^{*} Note that in all three cases explored here the BH binary orbit has been assumed to have negligible eccentricity.

[†] For the choice of the initial BH spin values see Section 2.6.

BH spins are allowed to be anywhere between 0 and 1. In this case the recoil BH remnant velocity can be computed as follows (Campanelli et al. (2007); Baker et al. (2008) see also Herrmann et al. (2007); Koppitz et al. (2007)):

$$\mathbf{v}_{\text{align, kick}} = v_{\text{m, kick}} \hat{\mathbf{e}}_1 + v_{\perp} (\cos \xi \hat{\mathbf{e}}_1 + \sin \xi \hat{\mathbf{e}}_2), \quad (4)$$

with

$$v_{\perp} = H \frac{\eta^2}{1+q} (a_2 - qa_1). \quad (5)$$

Here $\hat{\mathbf{e}}_1$ and $\hat{\mathbf{e}}_2$ are orthogonal unit vectors in the orbital plane, and a_1 and a_2 are the dimensionless spin vectors of the two holes. ξ measures the angle between unequal mass and spin contribution to the kick velocity. For simplicity, we assume ξ to be 90° , very similar to the value of 88° found by Campanelli et al. (2007), although this value is intrinsically very difficult to determine in numerical relativity simulations due to the strong precession of the spins near the merger. We adopt a value of $\sim 7.3 \times 10^3$ for the parameter H , as in Campanelli et al. (2007), while q and η have the same meaning as in the previous case. Note that in the case of mutually anti-aligned and maximally spinning BHs, the maximum kick velocity of order 460 km s^{-1} occurs for equal mass mergers.

2.4.3 Recoils for arbitrary mass ratio and random spin orientations

In our last and most general scenario, we consider mergers of binary BHs where the mass ratio, the spin magnitude and the spin orientations are arbitrary. We follow Campanelli et al. (2007) (see also Baker et al., 2008, for a somewhat lower maximum kick velocity estimate) and express the recoil velocity through a generalisation of the previous case, i.e.

$$\mathbf{v}_{\text{rand, kick}} = v_{\text{m, kick}} \hat{\mathbf{e}}_1 + v_{\perp} (\cos \xi \hat{\mathbf{e}}_1 + \sin \xi \hat{\mathbf{e}}_2) + v_{\parallel} \hat{\mathbf{e}}_z. \quad (6)$$

Note that for calculating v_{\perp} we need to consider only the components of the spin vectors along the orbital angular momentum. Instead, v_{\parallel} is given by

$$v_{\parallel} = K \cos(\Theta - \Theta_0) \frac{\eta^2}{1+q} (a_2^{\perp} - qa_1^{\perp}), \quad (7)$$

where $K = 6 \times 10^4$, $\Theta_0 = 0.184$, and the symbol \perp refers to the direction perpendicular to the orbital angular momentum. Θ is defined as the angle between $a_2^{\perp} - qa_1^{\perp}$ and the infall direction at the merger, which we consider to be a random variable.

In the case of arbitrary spin orientations, the maximal kick velocities occur when both spins lie in the orbital plane and are anti-aligned, and reach up to 4000 km s^{-1} for maximally spinning BHs. Thus, this case appears most dangerous for retaining BHs in the centre of host galaxies after a merger. Note, however, that even if such an unlikely merger configuration occurs, the probability of receiving a kick of that order of magnitude is further reduced due to the parameter Θ .

2.5 Numerical issues

Due to the nevertheless limited mass resolution of our cosmological simulations (see Section 3), even in our highest resolution runs the dark matter and gas particle masses are comparable to the BH seed mass. This implies that if a low-mass BH receives a recoil kick that is lower than the escape velocity from its host halo, the subsequent evolution of the BH's orbit would be computed inaccurately in the simulation, due to a misrepresentation of the dynamical friction forces. As a result, a recoiled BH would artificially wander through its host halo for a long time.

In order to correct for this effect one could try to explicitly estimate the dynamical friction time of a displaced BH, and then gradually reposition it over this timescale towards the centre of the halo. However, the orbit of the BH during the approach to the halo's centre would still have to be chosen arbitrarily. We therefore adopt here a much simpler model. Recall that we are primarily interested in the question whether a remnant BH will leave its host halo or not, and to what extent such expulsions can affect the growth of the first bright quasars. For our purposes it is therefore sufficient to compare the BH's kick velocity at the moment of the merger to the local escape velocity from its current host halo. If the former is larger, we give the correct kick velocity to the BH and follow its dynamical orbit that will carry it out of the halo (later re-accretion onto a more massive dark halo is however possible). In the opposite case, we simply neglect the small recoil that the BH would have received and do not alter its velocity. This approximation hence assumes that the displaced BH will return to the halo centre on a negligible time scale. In order to estimate the local escape velocity from the host halo, we assume a singular isothermal sphere profile for the halo. This effectively provides an upper limit to the number of BHs that are actually kicked out.

2.6 BH spin evolution due to the mergers

Given that even a merger of non-spinning BHs produces significant final BH spins, and that spins play an important role in determining the magnitude of the recoil velocity, it is prudent to consider BHs characterised by a non-vanishing spin and to account for spin evolution. Here we implement a basic model for the treatment of BH spins. Initially, when a dark matter halo is seeded with a small mass BH, we not only assign an initial mass to the BH but also a certain amount of spin that can range from 0 to 1. For simplicity, we assume that all BH seeds are characterised by the same initial spin value, and we perform several simulations where we vary the choice for the initial spin in order to understand how the subsequent evolution of the BH population depends on this parameter. Furthermore, when two BHs merge we estimate the final spin of the BH remnant on the basis of analytical fits to the numerical relativity calculations of Rezzolla et al. (2008c,b,a). This allows us to consider both the initial spin values of the two BHs prior to the merger as well as their configuration (either aligned/anti-aligned spins, or randomly orientated spins) to accurately estimate a final spin value. We can also follow spin flip events and estimate how often they occur during the cosmological BH growth. Finally, we perform additional ‘‘control’’ runs where we keep

Simulation	$N_{\text{HR}}/N_{\text{gas}}$	$m_{\text{DM}} [h^{-1}\text{M}_{\odot}]$	$m_{\text{gas}} [h^{-1}\text{M}_{\odot}]$	z_{start}	z_{end}	$\epsilon [h^{-1}\text{kpc}]$	$R_{\text{HR}} [h^{-1}\text{Mpc}]$
zoom5	1364500	6.75×10^6	1.32×10^6	127	6.2	1.0	3.4
zoom8	5588992	1.65×10^6	0.32×10^6	127	6.2	0.625	3.4
zoom10	10916000	0.84×10^6	0.16×10^6	127	6.2	0.5	3.4
zoom5_z4	21090625	6.75×10^6	1.32×10^6	127	3.9	1.0	8.4
zoom8_z4	86387200	1.65×10^6	0.32×10^6	127	5.3	0.625	8.4
zoom5_z2	99712125	6.75×10^6	1.32×10^6	127	2.1	1.0	14.0

Table 1. Numerical parameters of the cosmological galaxy cluster simulations analysed in this study. The names of the various runs performed are given in the first column, where zoom# indicates #³ higher mass resolution than the parent Millennium simulation. Rows four and five represent resimulations of the main descendent of our $z = 6$ halo that has been selected at $z = 4$, while in the last row we have selected for resimulation the main descendent at $z = 2$. The values listed from the second to the fourth column refer to the numbers and masses of the high-resolution dark matter and gas particles. Note that the actual values of N_{gas} and m_{gas} vary in time due to star formation. The last four columns give the initial and final redshifts of the runs, the gravitational softening length ϵ , and the radius of the roughly spherical high resolution region, respectively.

the BH spins constant and equal to their initial value, for comparison.

Note that in this study we do not take into account spin changes due to gas accretion, a process that could in principle be very important. We here refrain from attempting to model this physical process due to its intrinsic complexity and uncertainty, given that it is possible that gas accretion episodes lead either to spin-up or to spin-down of BHs (e.g. Volonteri & Rees, 2005; King & Pringle, 2006), depending on the nature of the accretion flow. However, by exploring a large range of initial BH spin values we can still gain some insight into a possible modification of typical BH mass accretion histories if, for example, extended episodes of gas accretion would lead to rapidly spinning BHs. An investigation of a spin evolution driven by gas accretion through suitable simulation sub-grid models is an interesting subject for future work.

2.7 Spin-dependent radiative efficiencies

In our new BH model, we can self-consistently account for the different efficiency of spinning BHs for turning the gravitational binding energy of an accretion flow into radiation. Spin-dependent radiative efficiencies will both change the amount of material that can be accreted onto a hole as well as modify the amount of feedback energy that is released. For standard accretion disks the radiative efficiencies of accreting BHs can vary from 0.057 for a non-spinning BH to 0.42 for a maximally spinning BH, thus possibly causing a large effect on the early growth history of BHs (Shapiro, 2005; Volonteri & Rees, 2006). Following Bardeen et al. (1972), we estimate the radiative efficiency at the innermost stable co-rotating circular orbit as

$$\epsilon_{\text{max}} = 1 - \frac{\tilde{r} - 2 + a/\sqrt{\tilde{r}}}{\sqrt{\tilde{r}^2 - 3\tilde{r} + 2a\sqrt{\tilde{r}}}}, \quad (8)$$

where

$$\tilde{r} = 3 + A_2 - \sqrt{(3 - A_1)(3 + A_1 + 2A_2)}, \quad (9)$$

$$A_1 = 1 + (1 - a^2)^{1/3} [(1 + a)^{1/3} + (1 - a)^{1/3}], \quad (10)$$

and

$$A_2 = \sqrt{3a^2 + A_1^2}. \quad (11)$$

Here a denotes the dimensionless BH spin, and the radius of the innermost stable co-rotating circular orbit is given by the product of \tilde{r} and the BH's total gravitational mass.

3 NUMERICAL SIMULATIONS

We have performed a suite of numerical simulations especially designed to address the issue of early BH growth. For this purpose, one ideally needs to simulate both an extremely large volume of the Universe of order of $0.5 - 1$ Gpc cubed, as the space density of high-redshift luminous quasars is very low, and at the same time reach a very large dynamic range in order to resolve at least \sim kpc scales reliably. Simulations that reach this resolution throughout such large volumes are currently beyond the reach of any state-of-the-art cosmological code, especially when gas and BH physics are included as essential ingredients.

We have therefore adopted a different approach that directly focuses on rare high density peaks (see e.g. Gao et al., 2005), where the first SMBHs are most likely to form. By restricting the region that needs to be resolved with high resolution to a small fraction of the total simulated volume we can reach sufficient resolution for numerically converged and meaningful results. The identification of a suitable target region requires a homogeneously resolved high-resolution parent simulation. For this purpose we use the dark matter-only Millennium simulation (Springel et al., 2005a), which has a volume of $(500 h^{-1}\text{Mpc})^3$, just large enough to expect about one luminous quasar at $z = 6$ in the simulation box, given the observed space density of the high-redshift SDSS quasars, and their probably high duty cycle (Shankar et al., 2008). For our primary simulations, we have selected the most massive dark matter halo formed at this epoch and resimulated it at much higher mass and force resolution. We note that this target dark matter halo is part of a protocluster region that collapses to a very rich cluster of galaxies by redshift $z = 0$ (Springel et al., 2005a).

The resimulations were performed by selecting the Lagrangian region of our target halo in the original initial conditions and by populating it with a larger number of lower mass particles, adding in additional small scale power up to the new Nyquist frequency, as appropriate. Around this high-resolution region, the mass resolution has been progres-

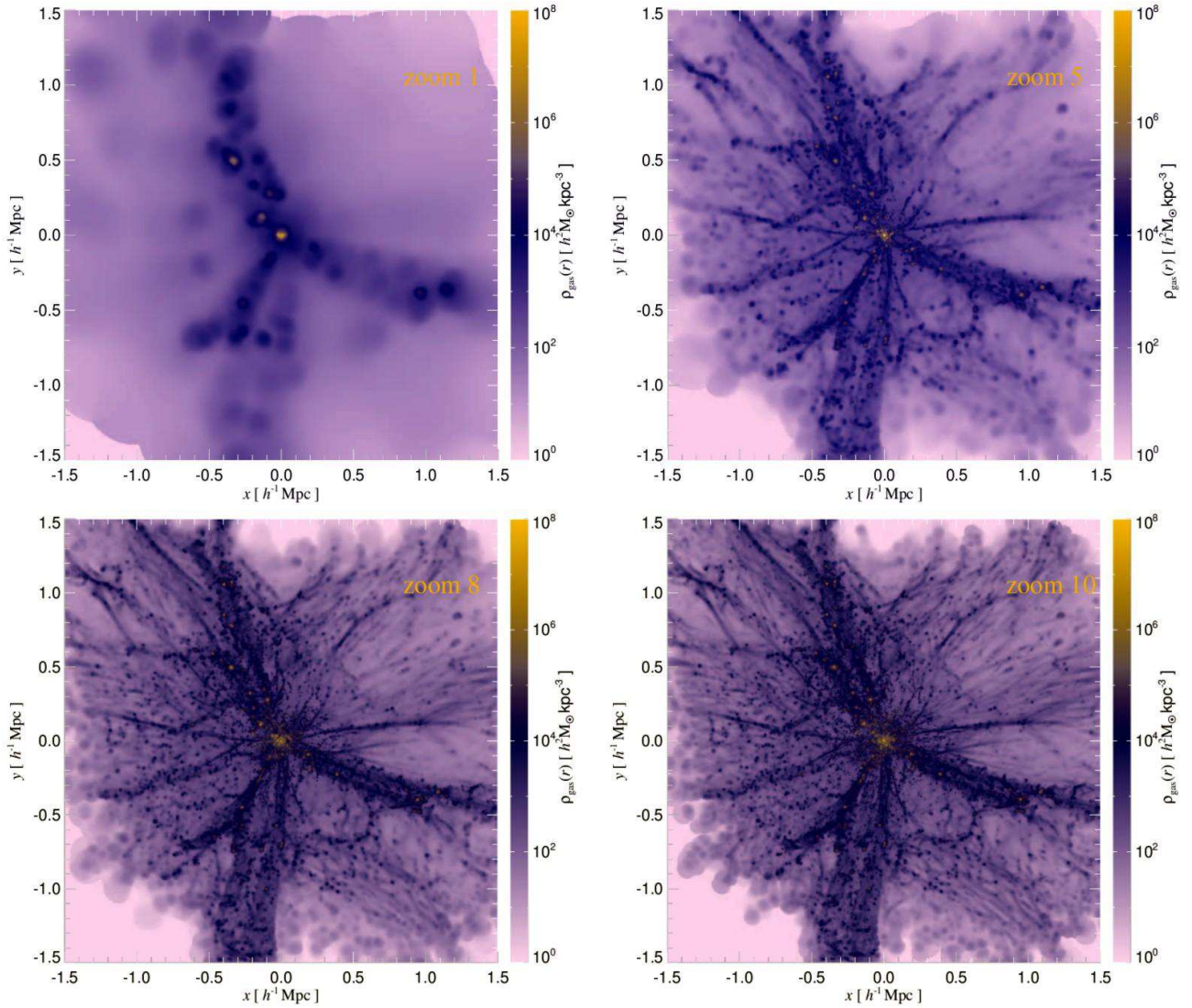


Figure 1. Projected mass-weighted gas density maps of the most massive $z = 6.2$ halo ($M_{200} = 4.86 \times 10^{12} h^{-1} M_{\odot}$) from the Millennium simulation, which was selected for resimulation. The upper-left panel shows the halo simulated with the resimulation technique with the same spatial and mass resolution as in the parent Millennium run. The remaining panels illustrate the same halo resimulated with 5^3 , 8^3 , and 10^3 times higher mass resolution, as indicated on the panels.

sively deteriorated by using ever more massive particles at larger distances, but making sure that the large-scale gravitational tidal field acting on the high-resolution region remained accurately represented. In order to test our resimulation setup, we have performed several dark matter-only simulations, verifying that the mass of the original target halo is reproduced accurately to within 1–2%. For the simulations with gas, we have split each high-resolution dark matter particle into a dark matter and gas particle, displacing them by half of the original mean inter-particle separation while keeping the centre-of-mass of each pair fixed. In this way the initial particle loads of dark matter and gas stay spatially separate as long as possible until the first non-linear structures form.

Based on the initial conditions constructed in this way we have performed a number of runs including gas, stellar and BH physics. We have additionally performed pure cooling and star formation runs, in order to gauge the impact of

BH feedback effects. We have further resimulated our $z = 6$ target halo at a number of different numerical resolutions, starting from a mass resolution of a factor 5^3 higher than the original Millennium run up to 10^3 times higher mass resolution. In Table 1, we summarize the main numerical parameters of our simulation suite. Moreover, in order to continue our simulations below $z = 6$, we have identified the main descendent of our $z = 6$ halo both at $z = 4$ and $z = 2$ in the original Millennium run, and resimulated those as well, starting again from a redshift of $z = 127$.

The cosmological parameters adopted in this study are the same as in the Millennium simulation, namely: $\Omega_m = 0.25$, $\Omega_{\Lambda} = 0.75$, $\sigma_8 = 0.9$, $h = 0.73$ and $n_s = 1.0$, corresponding to a flat Λ CDM cosmological model. We chose $\Omega_b = 0.041$ in order to reproduce the cosmic baryon fraction inferred from the most recent cosmological constraints (Komatsu et al., 2009).

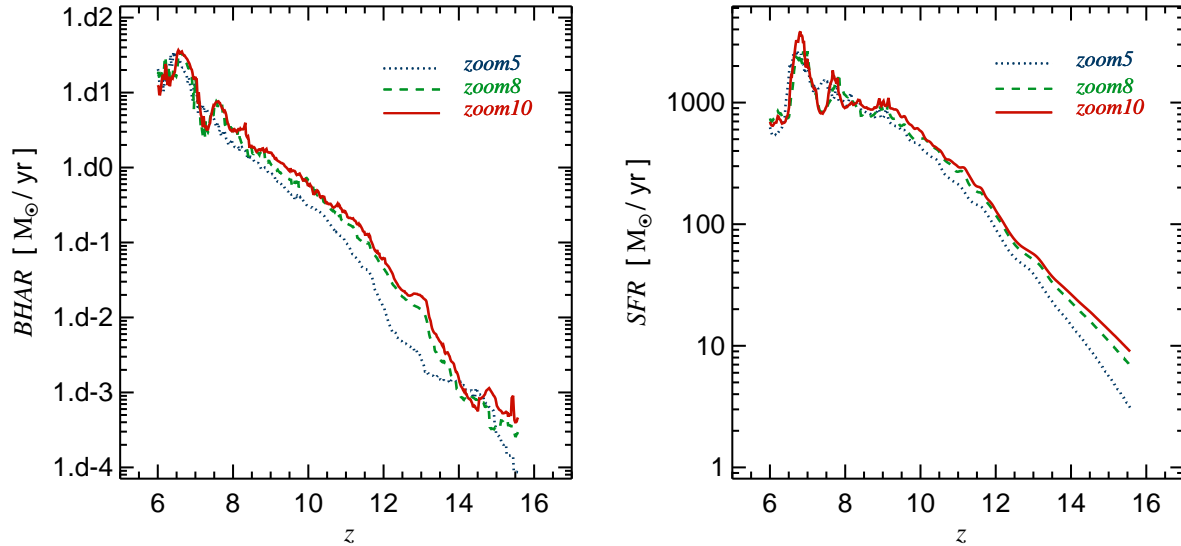


Figure 2. BH accretion rate (left-hand panel) and SFR (right-hand panel) in the simulated volume as a function of redshift. The different curves are for the same simulation performed at different numerical resolutions, increasing the mass resolution by up to a factor of 8. The BHs have been seeded here in haloes with masses above $10^9 h^{-1} M_{\odot}$. Reasonable numerical convergence in these quantities has been reached.

4 REPRODUCING HIGH-REDSHIFT QUASARS

4.1 Numerical convergence tests

We start our analysis with a series of resimulations of the $z = 6$ target halo[‡] using our default BH model. We systematically vary the numerical resolution by considering progressively improved spatial and mass resolutions that are 5^3 , 8^3 and 10^3 times better than the original Millennium simulation. This allows an assessment of the numerical convergence of our results. In Figure 1, we show the gas density distribution of our target halo for different resimulation runs with increasing resolution. The global properties of the resimulated halo are very similar in all the simulations performed (e.g. with respect to the position of the most prominent filaments ending up in the main halo; the sites of very dense gas that is subject to star formation, etc.). However, the richness of structures surrounding our target halo and the fine features in its interior are clearly much better represented in our higher resolution runs. In these simulations, a vast number of small haloes in the outskirts of the main system and a network of fine filaments between them is revealed. We note however that the zoom8 and zoom10 runs show almost identical gas density distributions.

Previously, we have already demonstrated good numerical convergence of our BH model in full cosmological simulations (Sijacki et al., 2007), but properly resolving the very early growth of BHs is particularly challenging. This requires that the host haloes at $z \sim 15$, when the first BHs start to be seeded, have to be represented by a sufficient number of particles such that the BH accretion processes can be followed accurately even at this early time. It is important to

note that if the resolution in these first host systems is too poor this will likely lead to an underestimated BH accretion rate, causing an artificial delay of the mass assembly of the first massive BHs. To avoid this numerical problem it is necessary to push the numerical resolution high enough to resolve the first BH hosts adequately. This also implies that the actually realized resolution imposes a natural limit on the minimum host halo mass that can reliably be seeded in our scheme.

Based on the numerical resolution experiments we have performed we find that a mass resolution of at least 5^3 times higher than the Millennium run is needed when BHs are seeded at the centres of $10^9 h^{-1} M_{\odot}$ haloes. This is illustrated in Figure 2, where we plot the total BH accretion rate (left-hand panel) and star formation rate (SFR; right-hand panel) as a function of time for our three high resolution runs (as indicated in the legend). Note that while the zoom5 run somewhat underpredicts the BH accretion rate and SFR at high redshifts, as expected given that a fraction of small haloes remains poorly resolved in this run, it has very similar BH accretion rate and SFR values for $z < 9$ compared with the zoom8 and zoom10 runs. On the other hand, the BH accretion rate and SFR of the zoom8 and zoom10 simulations are basically indistinguishable, indicating that we have resolved the bulk of the star formation and BH accretion occurring in the haloes within the simulated timespan.

In Figure 3, we analyze the mass growth of the most massive BH in these three runs of increasing resolution. For the zoom5 run the BH mass is again somewhat underpredicted at high redshifts with respect to the higher resolution simulations. At $z \sim 7 - 8$ the BH accretion rate in the zoom5 simulation comparatively increases, and the BH mass catches up with the values obtained for the zoom8/zoom10 runs. Contrary to what one may naively expect, we note that

[‡] See Table 2 for a list of its main properties.

MAIN HALO PROPERTIES AT $z = 6.2$												
Run	N_{200}	$N_{200,DM}$	$N_{200,gas}$	R_{200} [kpc/h]	M_{200} [M_{\odot}/h]	$M_{200,DM}$ [M_{\odot}/h]	$M_{200,gas}$ [M_{\odot}/h]	$M_{200,*}$ [M_{\odot}/h]	T_{200} [K]	SFR [M_{\odot}/yr]	M_{BH} [M_{\odot}/h]	M_{Edd}
no BHs	6436930	2475953	1047133	437.1	4.86×10^{12}	4.08×10^{12}	3.02×10^{11}	4.71×10^{11}	5.8×10^6	1820	–	–
with BHs	6206304	2491315	1468049	437.5	4.87×10^{12}	4.11×10^{12}	3.97×10^{11}	3.63×10^{11}	6.5×10^6	508	2.01×10^9	0.27

Table 2. The main properties of our resimulated halo at $z = 6.2$. The upper row refers to the run performed without BHs while the bottom row is for the simulation including BH growth and feedback, where BHs were seeded in haloes above $10^9 h^{-1} M_{\odot}$. Both simulations have been performed with a zoom factor of 8. The second to the fourth columns give the total, dark matter, and gas particle number within the virial radius (fifth column). The total, dark matter, gas, and stellar mass of the halo are listed in columns six to nine. The mean mass-weighted temperature and total star formation rate within the virial radius are given in columns ten and eleven, respectively. The last two columns report the central BH mass and its accretion rate in Eddington units.

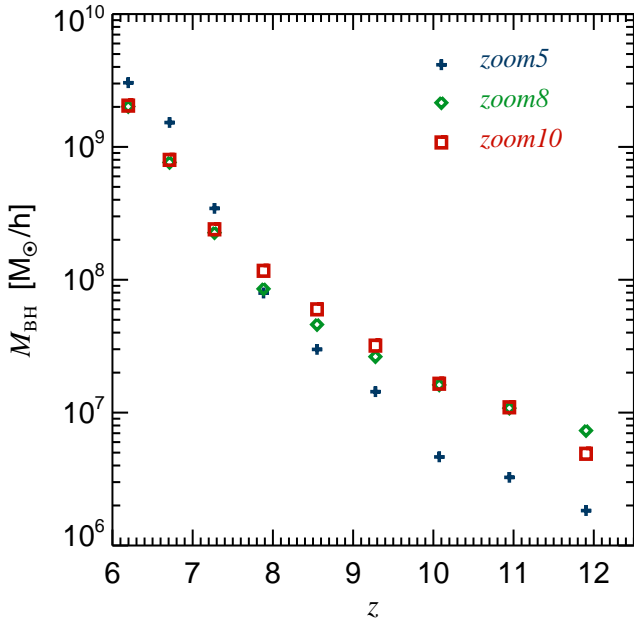


Figure 3. The mass of the most massive BH in the simulated volume as a function of redshift for the same runs as in Figure 2. While the zoom5 simulation somewhat underpredicts the BH mass at high redshift, for $z < 8$ it catches up with the higher resolution runs shown. The BH mass and accretion rate of the zoom8 run are basically indistinguishable from the zoom10 values, indicating robustness of our results.

this relative BH accretion rate increase in the zoom5 run for $z \sim 7-8$ does not lead to an overprediction of the BH masses for $z < 6$ (see Section 5 for a detailed description of the BH evolution at lower redshifts). The BH masses and hence BH accretion rates of the zoom8 and zoom10 runs are essentially identical at all redshifts, indicating that our estimates of the BH mass and the accretion rate onto our most massive BH have converged and are reliable. We have therefore decided to perform most of the simulations at the resolution of the zoom8 run for our further analysis. The only exception are the simulations we performed to much lower final redshifts of

$z = 4$ and $z = 2$. For computational reasons we have lowered for these the resolution to that corresponding to the zoom5 run. While this leads to a small delay in the BH growth at very high redshift, this bias becomes negligible at lower redshift, ensuring that the BH properties are well resolved and converged.

Our numerical tests highlight that even with the quite high resolution achieved here, we cannot reliably track BH seeds that start out in haloes as small as, e.g., $10^8 h^{-1} M_{\odot}$ haloes. Our choice for the mass-scale of the haloes we seed is thus in part determined by numerical limitations. In order to track BH growth in still smaller mass systems it would be necessary to construct dedicated simulations where the required still higher resolution can be reached. This would have to be accomplished at the expense of either choosing a smaller mass host halo at $z = 6$ for resimulation, or by restricting the simulations to cosmic structures at $z \gg 6$. Both of these are beyond the scope of this work. We therefore caution that our results rely on the assumption that the BH seeding process actually occurs within the haloes we can resolve, or that a population of BH seeds present at some earlier redshift is compatible with the BH seed population as we introduce it in our simulations.

Finally, Figure 3 shows that in our default BH model it is possible to produce a SMBH at $z \sim 6$ with a mass of $2 - 3 \times 10^9 h^{-1} M_{\odot}$ – within the range of the observational estimates of SDSS $z \sim 6$ quasars (e.g. Willott et al., 2003; Barth et al., 2003; Jiang et al., 2006; Kurk et al., 2007)[§]. Even though the BH growth starts from relatively massive seeds in our simulations this result is *non-trivial*. This is the first time that it is verified in full cosmological simulations of structure formation that there is sufficient gas available to fuel BH accretion and thus to build up such extremely massive BH in less than a Gyr of cosmic time. In previous work, Li et al. (2007) had employed a sequence of multiple mergers of isolated gas-rich spiral galaxies to show that such

[§] We have also checked explicitly how sensitive our results are to different choices of α , and found that even with $\alpha = 1$ (which is clearly suppressing the Bondi rate in the simulations), a SMBH of $9.9 \times 10^8 h^{-1} M_{\odot}$ is produced by $z = 6.2$, which is a factor of ~ 2 lower than the mass of the SMBH with $\alpha = 100$, adopting the same numerical resolution.

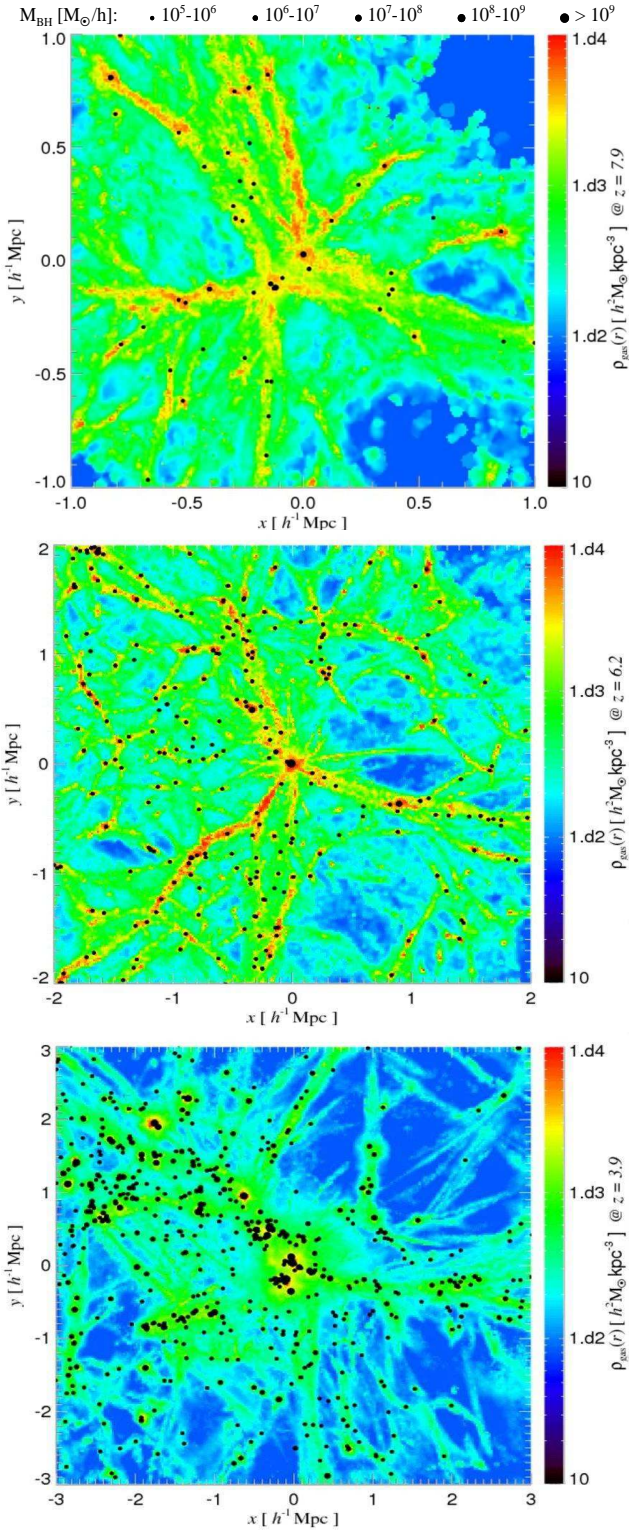


Figure 4. Projected mass-weighted gas density maps of the most massive Millennium halo at $z = 6.2$, resimulated at much higher resolution with gas and BHs. The middle panel shows the large-scale environment of the halo at $z = 6.2$. The upper and lower panels show the main progenitor and the main descendent of this halo at $z = 7.9$ and $z = 3.9$, respectively. The black dots denote the positions of BH particles, with their size encoding the BH mass as indicated on the legend. Note that at $z = 7.9$ two already very massive BHs in the centre of their respective host haloes are about to undergo a merger and thus contribute to the build-up of the SMBH at $z = 6.2$.

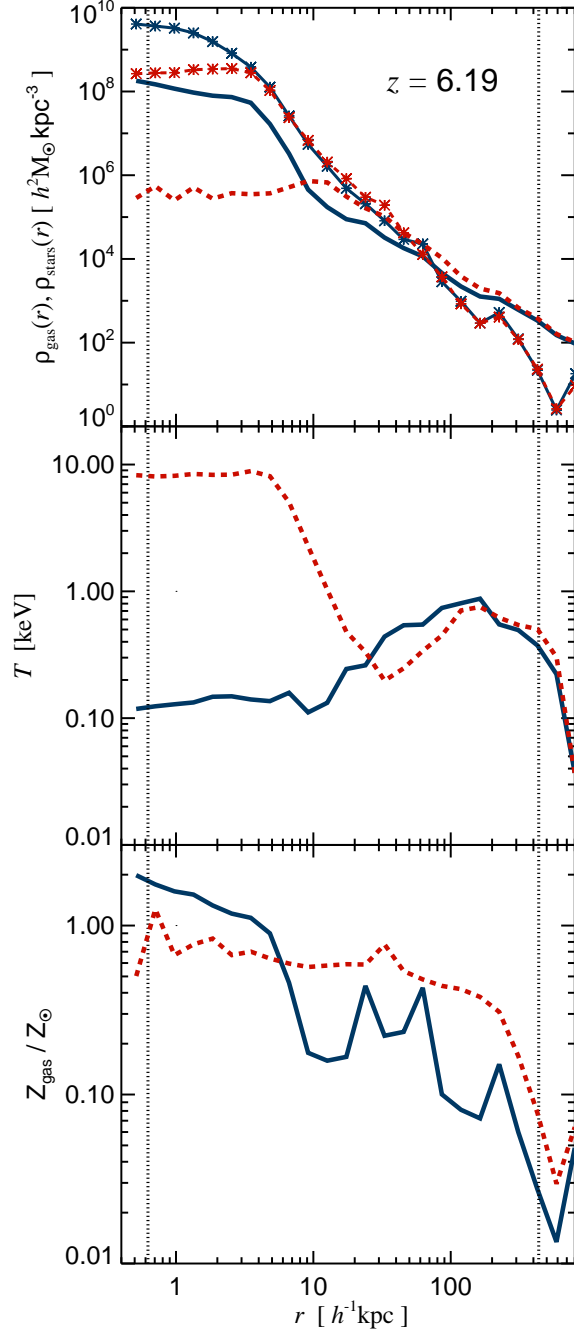


Figure 5. Radial profiles of gas density, mass-weighted temperature and mass-weighted gas metallicity of the most massive halo at $z = 6.2$ for a run without BHs (blue continuous lines) and for the simulation where BH are included (red dashed lines). In the top panel stellar density profiles are shown as well (denoted with star symbols with the same colour coding and line styles). Both simulations have been performed with a zoom factor of 8, and BHs were seeded in haloes above $10^9 h^{-1} M_{\odot}$. The vertical dotted lines denote the adopted gravitational softening length and the virial radius of the halo (in comoving units). The dramatic effect of the powerful quasar feedback on the properties of the host halo can be clearly seen: the central gas density is lowered by ~ 2 orders of magnitude and the temperature is increased by a similar amount.

rapid growth appears possible in principle. We here confirm that this is indeed the case when the full cosmological context is modelled self-consistently. Moreover we are finding in our simulations that the SMBH is produced only in the centre of the most massive halo, thus further corroborating our assumption that such rare and massive haloes are appropriate hosts for the SDSS quasars. Our formation scenario is also in good agreement with the estimated comoving space density of the SDSS quasars.

4.2 The supermassive BH and its host at $z = 6$

In Table 2 we list the main properties of our target halo at $z = 6.2$ for simulations with and without BHs. Comparison reveals the significant effect of the AGN feedback on the halo properties. In the last two columns we give the central BH mass and the accretion rate in Eddington units. The star formation rate is reduced by a factor of ~ 3 due to the AGN feedback. AGN heating starts to reduce the amount of stars formed from $z \sim 12$. Hence, the stellar mass of the host halo is decreased by $\sim 23\%$, while the amount of gas within the virial radius is larger by $\sim 31\%$. We note however that the total baryonic mass within the virial radius up to $z = 6.2$ is very similar in both runs. At $z \geq 6.2$ quasar activity mostly affects how much gas will cool and form stars, but it is not capable of expelling large quantities of baryons from the host halo. Table 2 further shows that the mean gas temperature within the virial radius is higher in the run with BHs, a clear signature of the thermal AGN feedback which generates very hot gas in the central regions of the halo, as we will discuss in more detail later on.

In Figure 4, we show projected mass-weighted density maps of our resimulated halo at three different redshifts, $z = 7.9$ (top panel), $z = 6.2$ (middle panel), and $z = 3.9$ (bottom panel). The black dots indicate the positions of BH particles. The size of the symbols encodes information about their mass, as indicated in the legend. In the top panel the main progenitor of our $z = 6$ halo experiences a merger with a halo of similar size which contains another relatively massive BH in its core. By $z = 6.2$, the most massive halo appears fairly relaxed. It is the only one to contain a BH with mass above $10^9 h^{-1} M_\odot$ in its centre and is surrounded by an intricate web of filaments containing many smaller haloes and actively growing BHs. By $z = 3.9$, our target halo has grown considerably in mass and is once more strongly perturbed due to several merging events. There are now also several smaller mass haloes with BHs with masses above $10^9 h^{-1} M_\odot$ in the vicinity. One of them is just in the process of merging with our target halo.

The effect of the AGN feedback on the properties of the host halo at $z \sim 6$ becomes apparent in Figure 5. We here plot radial profiles of the gas and stellar density, the mass-weighted temperature and the gas metallicity for the run without BHs (blue continuous lines) and with BHs (red dashed lines). The powerful quasar feedback significantly alters the gas and stellar properties, especially in the central regions of the halo. With AGN heating the gas temperature in the inner $20 h^{-1} \text{kpc}$ is increased by almost two orders of magnitude, while the gas density is reduced by a similar amount. At the same time, the distribution of metals becomes much more uniform throughout the host halo. The right-hand panel of Figure 6 gives a striking visual impres-

sion of the effect of AGN feedback on the gas metallicity distribution, which is shown for a simulation without BHs in the left-hand panel. During the epoch when the SMBH is growing rapidly the thermal feedback generates hot gas outflows which eventually shut down the BH accretion, resulting in self-regulated growth.

4.3 The influence of different halo threshold masses for BH seeding

In order to investigate how sensitive the mass growth of the most massive BH at $z = 6$ is to details of the adopted seeding procedure we compare two particular runs. In one, BHs were seeded within $10^9 h^{-1} M_\odot$ haloes, while in the other the BH seeds were introduced in more massive haloes of $10^{10} h^{-1} M_\odot$. All other parameters of these two simulations were kept the same. The simulations were run with a zoom factor of 8. Obviously, these tests do not cover the whole parameter space of possible seeding prescriptions. They provide us nevertheless with a good idea of how much, for example, mergers with other small mass BHs contribute to the build up of the most massive BH.

In Figure 7, we plot with the thick blue line the evolution of the main progenitor of the most massive BH at $z = 6$ in the run where BHs were seeded in $10^{10} h^{-1} M_\odot$ haloes (left-hand panel), and in the run where instead $10^9 h^{-1} M_\odot$ haloes were seeded (right-hand panel). The symbols and lines with different colours indicate the merging history of the secondary progenitors that merge with the main progenitor (see the caption of Figure 7 for further explanations).

The main progenitor in the simulation where the BH seeds are placed in smaller mass haloes is always more massive. At $z = 6$, this difference translates into the SMBH reaching $\sim 3 \times 10^9 h^{-1} M_\odot$ instead of $\sim 2 \times 10^9 h^{-1} M_\odot$. In order to better understand the cause of this mass difference, we have calculated the total mass of all BHs that have merged onto the main progenitor until $z = 6$. This number turns out to be $\sim 28\%$ and $\sim 6\%$, respectively. This means that in total the SMBH at $z = 6$ has increased its mass by $\sim 7 \times 10^8 h^{-1} M_\odot$ more due to BH mergers and by $\sim 3 \times 10^8 h^{-1} M_\odot$ more due to the gas accretion compared with the SMBH that has been seeded in the $10^{10} h^{-1} M_\odot$ halo. It should be stressed however that the mass difference of $\sim 7 \times 10^8 h^{-1} M_\odot$ due to BH mergers still for the most part comes from gas that has been accreted by secondary progenitors prior to the merger with the main progenitor. The total mass of all seeds that eventually end up in the SMBH is still very small with respect to its final mass, of the order of few %. This finding therefore supports the important conclusion that irrespective of the details of our seeding prescription, the main channel of mass growth of SMBHs is *gas accretion*.

In order to get a handle on the average efficiency of the BH accretion luminosity, ϵ_1 (or equivalently, on the average Eddington ratio assuming constant radiative efficiency ϵ_r) we adopt the following equation which characterises the BH growth due to accretion:

$$M_{\text{BH}}(t) = M_{\text{BH}}(t_0) \exp\left(\epsilon_1 \frac{1 - \epsilon_r}{\epsilon_r} \frac{(t - t_0)}{t_S}\right). \quad (12)$$

Here t_0 and t are the initial and final epochs that we identify with 0.35 and 1 Gyr, respectively, for this analysis, while

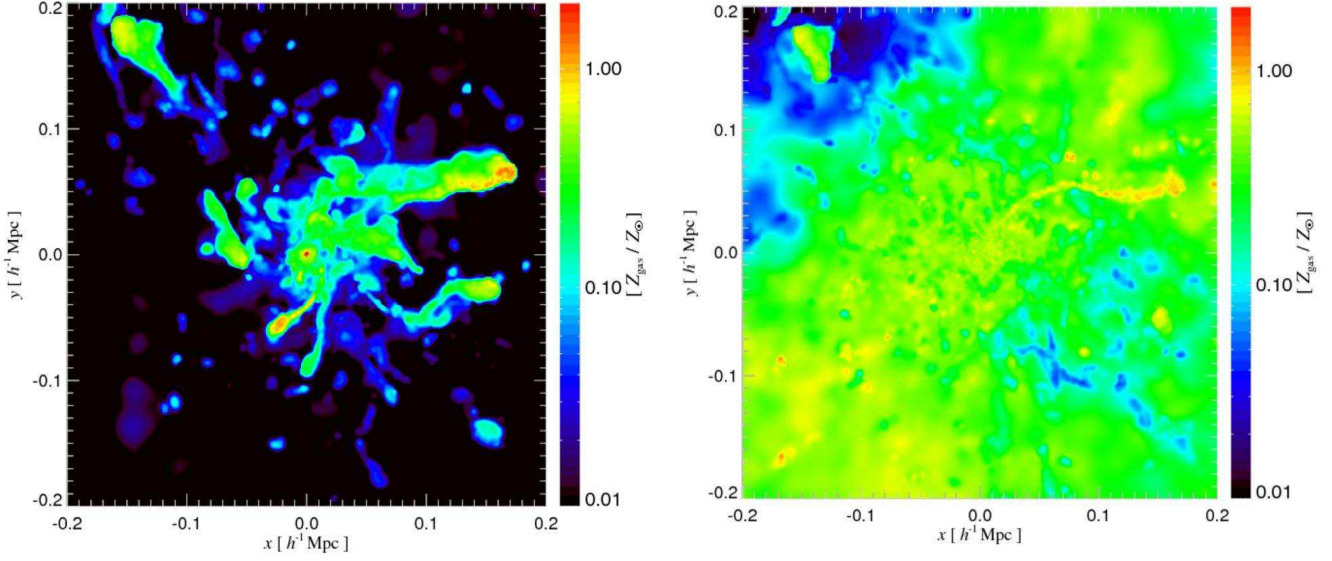


Figure 6. Projected mass-weighted metallicity maps of the central region of the most massive halo at $z = 6.2$. The left-hand panel shows the results of a simulation computed without BHs, while the right-hand panel is for a simulation with our default BH model. The metallicity distribution is significantly affected by quasar feedback. In the run with BHs, highly metal enriched gas is expelled from dense star forming regions, and spread out even out to distances of $400h^{-1}\text{kpc}$ from the central quasar. Note in particular the high metallicity trail, visible to the right. It is caused by a fly-by of a substructure and persists even in the presence of powerful AGN activity.

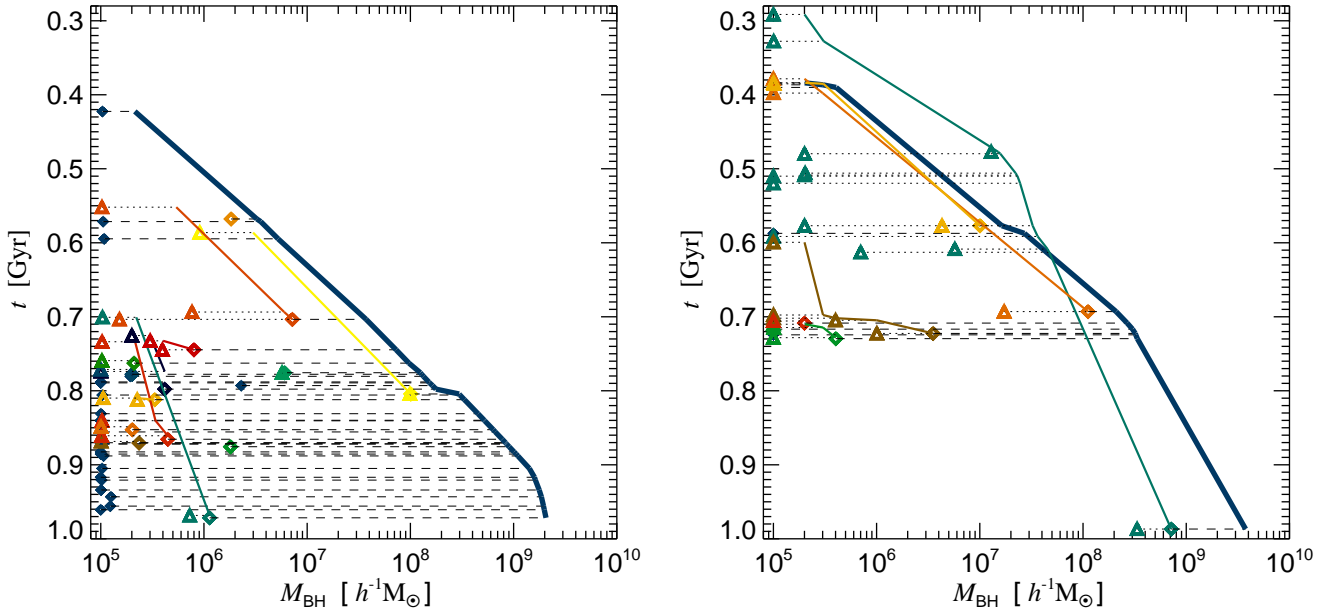


Figure 7. Merger tree of the most massive BH in the simulation at $z = 6$. The left-hand panel shows the merger tree for a simulation where BHs were seeded in $10^{10} h^{-1}M_{\odot}$ haloes, while the right-hand panel illustrates the case where the BHs were seeded in smaller haloes of $10^9 h^{-1}M_{\odot}$. Both runs have been performed with a zoom factor of 8. The blue thick line represents the main progenitor of the most massive BH at $z = 6$. The diamond symbols of different colour denote the mass of the second most massive progenitor, which merges with the main progenitor as indicated by the dashed lines. Blue coloured diamonds denote BHs that have never merged before. Thin continuous lines of different colour (matching the colour of the diamonds) show instead how the second progenitors of our main BH evolve with time. Finally, the triangles with matching colour indicate BHs that merge with the second progenitors of our main BH. BH seeding in smaller haloes causes significant changes in the BH merger history: most notably, BHs seeded earlier tend to be more massive at a given redshift. This is due to the combined effect of accretion and mergers.

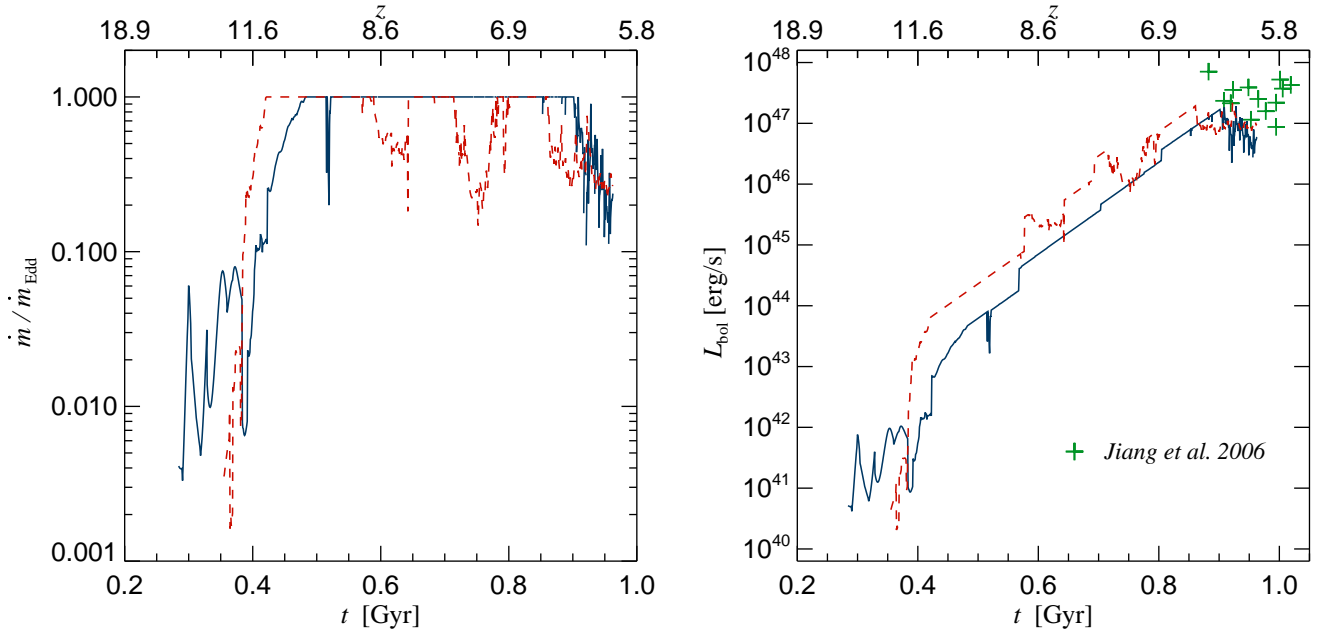


Figure 8. BH accretion rate in Eddington units (left-hand panel) and bolometric luminosity (right-hand panel) of the main progenitor of the most massive $z = 6$ BH. The blue continuous lines denote the run where BHs were seeded in $10^{10} h^{-1} M_{\odot}$ haloes, while red dashed lines are for the run where this threshold value has been reduced to $10^9 h^{-1} M_{\odot}$. The green cross symbols indicate observational estimates of L_{bol} for a sample of high redshift quasars by Jiang et al. (2006).

$M_{\text{BH}}(t_0)$ and $M_{\text{BH}}(t)$ are the BH masses at these two epochs, taken directly from our simulations (for $M_{\text{BH}}(t)$ we consider the total BH mass at epoch t accumulated by accretion only). The characteristic accretion timescale is given by the Salpeter time, t_S , that we assume to be equal to ~ 0.45 Gyr. Substituting these values in equation (12), we find that the average ϵ_l value is of the order of 0.8. This highlights that even though BHs experience extended episodes of Eddington-limited accretion in our model, it is still unlikely that BHs can accrete always close to the Eddington rate from very high redshift to the epoch of $z = 6$ quasars, as is often assumed in simple treatments.

In Figure 8 we illustrate how the accretion rate (left-hand panel) and the bolometric luminosity (right-hand panel) of our main progenitor evolve with time in the simulations where BHs were seeded in $10^9 h^{-1} M_{\odot}$ haloes (red dashed lines) and $10^{10} h^{-1} M_{\odot}$ haloes (blue continuous lines). At $t < 0.4$ Gyr, the BH’s main progenitor in the run with the lower halo threshold mass first undergoes three mergers with other BH seeds. Afterwards it starts accreting rapidly, soon reaching the Eddington limit. This leads to a head-start in the assembly of the main progenitor with respect to the simulation with the higher value of the halo mass threshold for BH seeding. For $t > 0.5$ Gyr, the BH which started rapid growth earlier (red dashed lines) experiences several extended sub-Eddington accretion episodes compared with the other run (blue continuous lines). However, in absolute terms its accretion rate is higher (as reflected by the bolometric luminosity). These sub-Eddington accretion episodes are related to a temporary exhaustion of the local gas reservoir available for accretion.

Finally, by $z \sim 6$, the most massive BHs in the two runs performed are characterized by similar bolometric luminosities

that we compare to observations (indicated by the green crosses). The observed values are taken from a recent paper by Jiang et al. (2006), who have performed Spitzer observations of 13 high redshift quasars and combined those results with observations ranging from X-ray to radio to get a more realistic estimate of the bolometric luminosities. Having simulated only one $z = 6$ quasar we cannot perform a detailed statistical comparison with observations; however, while our bolometric luminosity L_{bol} lies at the lower end of the observed range (note that observational error bars were not available), it is clearly consistent with the observed values.

4.4 Can galactic winds stall the initial growth of BHs?

Given that gas accretion drives the growth of massive BHs at $z = 6$, it is interesting to consider possible physical mechanisms that we have not taken into account so far and that could in principle impede BH accretion and thus stall BH growth. Note that the BH feedback itself, which is already part of our default model, does not prevent BHs from becoming supermassive. However, the situation may be different if the BH feedback effects are in reality much stronger than what we have assumed in our simulations thus far, a possibility that we examine further in Section 4.6, when we discuss rapidly spinning BHs. Another possibility is stronger feedback associated with star formation, which could also deprive BHs of the gas for accretion. We here examine galactic winds from star formation as one possibility of such strong feedback.

There is good observational evidence that many host galaxies of SDSS quasars experience a very high level of star formation of the order of $\sim 1000 M_{\odot} \text{ yr}^{-1}$ (e.g. Bertoldi

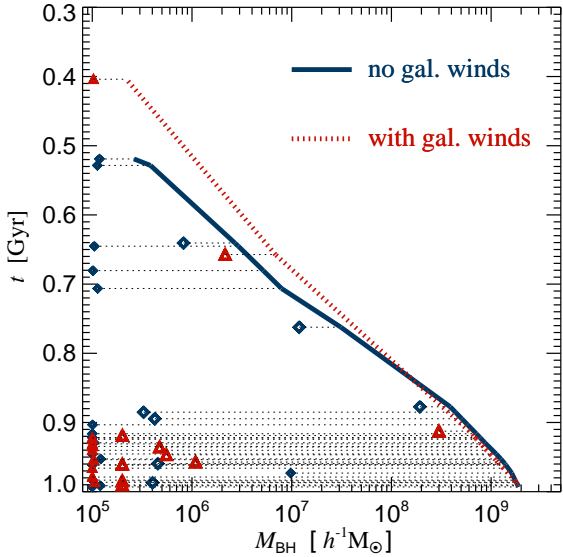


Figure 9. Merger tree of the most massive BH at $z = 6$ in simulations with (red dashed line and triangles) and without (blue continuous line and diamonds) galactic winds. Both simulations have been performed with a zoom factor of 5. The continuous lines show how the mass of the BH’s first progenitor grows with time while the symbols represent secondary progenitors that merge onto it, as indicated by the dotted lines. Galactic winds have no significant impact on the merger tree of the most massive BH throughout the whole simulated time span.

et al., 2003; Carilli et al., 2004; Wang et al., 2008). Starburst-driven galactic winds are therefore an obvious physical process that could significantly deplete the amount of gas available for accretion onto massive BHs in these systems. In order to explore such a scenario, we have performed an additional test run (selecting zoom factor 5 this time) where we have ‘switched-on’ galactic winds as implemented by Springel & Hernquist (2003). The properties of the galactic outflows are determined by two parameters. The first is the wind velocity, which is constant regardless of the host galaxies’ mass. We select it to be rather high of order of $\sim 480 \text{ km s}^{-1}$. The second parameter regulates the mass loading factor of the wind, according to $\dot{M}_w = \eta \dot{M}_{\text{SFR}}$, where we choose η to be 2.

In Figure 9, we show the redshift evolution of the mass of the most massive progenitor of the $z = 6$ target BH, both without (blue continuous line) and with galactic winds (red dashed line). Note that apart from the inclusion of galactic winds, all other simulation parameters and the numerical resolution were kept exactly the same in both simulations. Figure 9 demonstrates that galactic winds have overall very little effect on the mass growth of the most massive BH. The rather limited efficiency of galactic winds to expel gas from the BH host halo (or to change gas thermodynamical properties significantly) is due to the combination of two factors. First, even though the chosen wind velocity from supernova feedback is rather high, at $z \sim 6 - 8$ it is comparable or even lower than the escape velocity of the host halo of the most massive BH, and thus galactic winds cannot unbind the gas from the halo. Second, regardless of the high wind efficiency

parameter η we have adopted, the amount of star formation occurring in the most massive BH host halo is not particularly high at high redshift. It only reaches the intense levels of $\sim 1000 M_{\odot} \text{ yr}^{-1}$ at $z < 9$, when the BH host halo has become sufficiently massive to prevent galactic winds from leaving the halo.

This result is in line with the findings of Li et al. (2007), who used the same wind model with similar wind speed (but lower wind efficiency parameter combined with higher SFRs of their simulated galaxies at high z). Hence, in order to prevent or considerably reduce massive BH growth at these high redshifts by means of starburst driven winds one would need to invoke a much more extreme kinetic feedback. Either the wind velocity would need to be significantly higher, e.g. $\sim 1000 \text{ km s}^{-1}$ (possibly combined with even higher wind efficiencies and/or higher SFRs of the host haloes). Or the nature of the wind would need to be more violent than assumed in our model, with much larger mass-loading factors that blow away a considerable fraction of the ISM around massive BHs. In any case the final wind velocities would need to be high in order to prevent that the blown away material falls back and feeds the BH after some delay. In other words, only a substantially larger kinetic luminosity of the winds may change the above conclusion.

4.5 Gravitational wave recoils and the growth of SMBHs at high z

Asymmetric gravitational wave emission during a BH merger carries away linear momentum, which in turn imparts a velocity kick on the remnant BH. Given that such induced BH kick velocities can have significant values amounting to thousands of kilometres per second, it is extremely interesting to consider their possible impact on the BH assembly in cosmological simulations, where we have direct knowledge when BHs are merging, which properties they have at the time they merge, and which haloes they are embedded in. If gravitational wave recoils frequently displace or expel BHs from the centres of their host haloes, this may have dire consequences for the build up of massive BHs at high redshift, possibly even obstructing the formation of SMBHs by $z = 6$ in the co-evolution scenario that we study.

It is one of the important goals of this study to better understand this question. For this purpose, we have extended our BH model and incorporated three scenarios for BH kicks, as described earlier. These can be labelled as the ‘mass asymmetry’, the ‘parallel spins’ and the ‘random spins’ parametrization of the kicks (see Section 2.4 for the detailed definitions).

Given that the most interesting range of kick velocities is obtained when BHs are spinning, we first assume, for definitiveness, that all BHs are characterized by the same initial spin parameter. We keep the BH spins constant with cosmic time and do not change the radiative efficiency as a function of the spin, in order to gauge more straightforwardly the impact of BH recoils on the BH assembly. For spin-dependent radiative efficiencies, see Section 4.6 below, while for the evolution of BH spins due to the mergers, see Section 4.7. As for the magnitude of the BH spins, we fix it at a rather high value of 0.9, but we also consider lower values of 0.3 and 0.5 to explore the parameter space. Obviously, in the case of mass-asymmetry kicks, we assume that

the BHs are spinless (as in our default model) and we do not change the spin magnitudes after a merger (as should be appropriate). This case serves as a lower limit for the effect of BH recoils.

For our three different scenarios for BH remnant recoils, we have performed a number of resimulations of our target $z = 6$ halo. In particular, we have both considered the case when the halo mass threshold value for BH seeding is $10^{10} h^{-1} M_{\odot}$ and when it is $10^9 h^{-1} M_{\odot}$. In the latter case, more seed BHs are introduced and hence more mergers with the main progenitor of the most massive BH occur (there are also more BH mergers overall), making this case more favourable for effects due to BH kicks. Nevertheless, regardless of the seeding prescription adopted, we find that BH kicks *cannot* prevent the build-up of the most massive BH, which reaches a mass of a few times $10^9 h^{-1} M_{\odot}$ even when we assume that all BHs are rapidly spinning (with a spin value of 0.9), and irrespective of the assumed orientation of BH spins at the merger. This is illustrated in the right-hand panel of Figure 12, where for the case of randomly oriented spins with $a = 0.9$ we plot the mass of the most massive BH formed in the simulated volume (magenta star symbols connected with dashed line).

In order to understand why BH kicks cannot stall the growth of massive BHs in our model we have computed a number of BH properties at the moment when they are about to undergo a merger. In Figure 10, we show in the left-hand panel the distribution of mass ratios of merging BH pairs over the whole simulated timespan (from $z \sim 15$ when the first BHs are formed to $z \sim 6$). Three different histograms (red dot-dashed lines: mass asymmetry kicks, blue continuous lines: parallel spins, and green dashed lines: random spins) illustrate the three scenarios we have adopted for BH recoils. The isolated peak to the right in the distribution corresponds to equal mass mergers and is mainly due to BHs close to their seed mass merging with each other. Apart from this feature, the distribution of mass ratios is broad and peaks at the value of 1 : 10, with mass ratios of 0.07 being as common as ratios of 0.2.

In the middle panel of Figure 10, we instead show the distribution of kick velocities of remnant BHs. The vertical arrows with matching colours and line styles denote the median values of the kick velocity distributions for the three cases considered. While for all three scenarios the distribution of kick velocities peaks at around $150 - 250 \text{ km s}^{-1}$, the maximum kick velocity is smallest for the mass asymmetry induced kicks, and largest for randomly oriented spins, as expected. The tail of the distribution at low kick velocities is more pronounced in the case of mass asymmetry kicks and for parallel spins, than for the run with random spins. This can be understood as follows. For the mass asymmetry kicks, the kick velocity will be very low both when the mass ratio is close to one and when it is very small, and will hence contribute to the tail of the distribution. Instead, in the case of parallel spins, given that the two BH spins can be aligned or anti-aligned with equal probability (recall that we are choosing their alignment with respect to the orbital angular momentum randomly), the contribution to the kick velocity will be zero when the alignment of the spins occurs. On the other hand, for the case of random spins, it is unlikely that the spins become mutually aligned and cause no kick, as we do not impose any constraints on the spin orien-

tation in this case. The variety of possible spin orientations in this case causes kick velocities that are higher on average. Finally, the shaded region in the middle panel of Figure 10 indicates the range of escape velocities from haloes when a BH merger occurs. This shows that in a number of mergers the BHs actually get kicked out from their host halo.

In order to better constrain the fraction of kicked out BHs, we show the distribution of the ratio of kick velocity to escape velocity from the host halo at the moment of the merger in the right-hand panel of Figure 10. All the mergers that populate the distribution to the right of the vertical black line can cause the remnant BH to get expelled. Thus, in all three kick scenarios explored here, there are BHs which experience kick-outs from their host halo, and the fraction of these events varies from 22% for mass asymmetry kicks, over 31% for parallel spin recoils, up to 36% for the case of randomly oriented spins. Therefore, the fraction of BHs kicked out from their host haloes is significant, ranging from about 20% if the BHs are not rapidly spinning to almost 40% if we assume that the whole population of BHs is instead characterized by a rather large spin value of 0.9.

However, the majority of these BHs that are expelled turn out to be fairly small mass BHs. To demonstrate this, in Figure 11 we show again the distribution of mass ratios (top panels) and kick over escape velocities (bottom panels), but this time imposing that at least one of the two merging BHs needs to be more massive than $5 \times 10^6 h^{-1} M_{\odot}$ (left-hand panels) or $5 \times 10^7 h^{-1} M_{\odot}$ (right-hand panels). From these panels we can deduce that more massive BHs are less likely to undergo a merger with a similar mass BH. While in the case of BHs more massive than $5 \times 10^6 h^{-1} M_{\odot}$ there are still some mergers that can cause the remnant to be kicked out of the host halo, for BHs more massive than $5 \times 10^7 h^{-1} M_{\odot}$ virtually no BH remnant has a sufficient kick velocity to escape from its host halo. Three factors contribute to this: similar mass mergers are quite rare, the probability of having BH spins oriented such that high enough kicks are produced is low, and as BHs grow in mass so do their host haloes and consequently the escape velocity increases. Combined, these effects imply that gravitational wave induced BH recoils *cannot* prevent the formation of SMBHs at high redshifts. This result is in line with our previous finding that most of the SMBH mass at $z = 6$ is assembled by gas accretion, and that BH mergers contribute only in a minor way to the hole's formation.

Nonetheless, we should stress that an important caveat for this result lies in our seeding prescription. In scenarios where BH seeds are present also in much smaller haloes than we have assumed and/or where BH seeding occurs at even higher redshifts than $z \sim 15$, it is likely that BH mergers will contribute much more to the mass assembly of early BHs. If in such scenarios BHs happen to be sufficiently spinning, gravitational wave recoils could have a much more damaging effect than we find here. Still, further direct modelling by means of numerical simulations is necessary to establish if this would indeed lead to a bottleneck for the early formation of SMBHs. Interestingly, if it can be shown that this should really be the case, then the fact that SMBHs *are observed* at $z = 6$ can be used to argue against such scenarios and be taken as indirect evidence that BHs at high redshift should have modest values of BH spins and/or that the majority

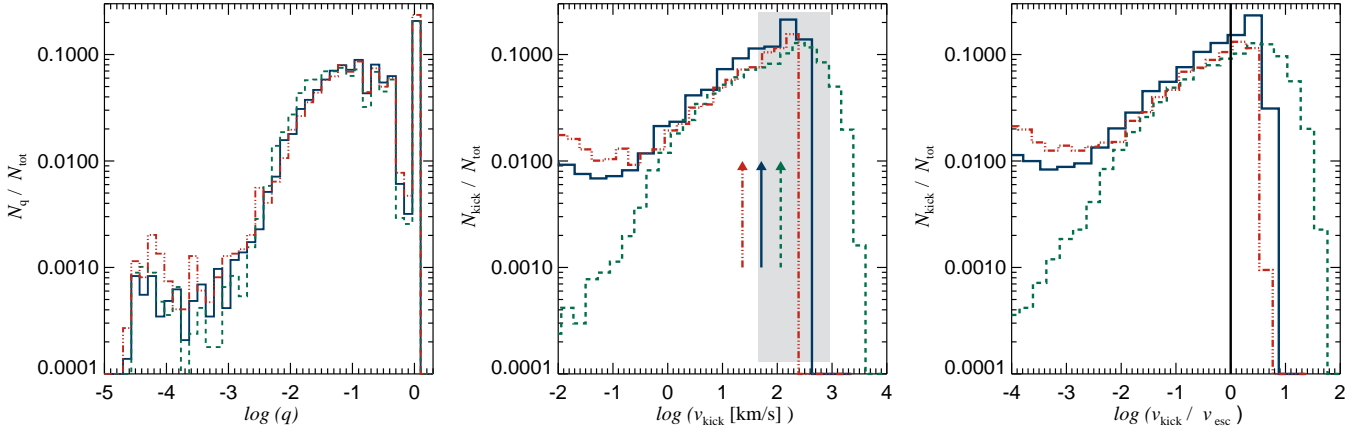


Figure 10. Distribution of mass ratios (left-hand panel), kick velocities (middle panel) and kick velocities divided by host halo escape velocities (right-hand panel) for all BH mergers at $z \geq 6$ for simulations with the three implementations of gravitational wave recoils. The red dot-dashed lines are for simulation where recoil kicks are only due to the mass asymmetry of merging BHs. The blue continuous lines are for the run where BH spins are always aligned or anti-aligned, and the spin magnitude is kept fixed at 0.5. The green dashed lines represent the case where the spin orientations are random and the spin magnitude is 0.9. In all three cases BHs are seeded in haloes with masses above $10^9 h^{-1} M_{\odot}$. The gray region in the middle panel denotes the range of escape velocities of haloes which host merging BHs. The vertical arrows with matching colours and line styles show the median value of the kick velocity distributions for the three cases considered.

of BH seeds should be formed in the centres of relatively massive dark matter hosts, as we have assumed in this work.

4.6 Spinning BHs with high radiative efficiency

Above we have shown that BH recoils cannot stall the growth of the most massive BHs in our simulations, even when they are characterized by a rather large spin value. However, we have not yet taken into account that the radiative efficiency is spin dependent. The spin dependent radiative efficiencies can modify both the amount of material that a hole can accrete (here we assume that the BH accretion is radiatively efficient, and not advection dominated) and thus also the amount of thermal feedback. Highly spinning BHs are expected to have radiative efficiencies approaching 0.42 (Bardeen et al., 1972; Thorne, 1974), and if indeed such a large fraction of the accreted rest mass energy is lost to radiation this can have a major impact onto the mass assembly of BHs.

In order to explore this possibility we have performed additional simulations where we kept the spins of all BHs constant, but where we have computed the radiative efficiencies from equation (8). In Figure 12, we show the mass of the most massive BH in the simulated volume as a function of redshift in the case where BHs were seeded in $10^{10} h^{-1} M_{\odot}$ haloes (left-hand panel) and in $10^9 h^{-1} M_{\odot}$ haloes (right-hand panel). Blue connected triangles denote the BH mass obtained from our default model. Green connected squares (only in the left-hand panel) are instead for the run where the BHs are spinless (as in our default model), but the radiative efficiency assumed is somewhat lower than in our default model (given by equation 8). Finally, the red connected diamonds illustrate the case where all BHs are rapidly spinning, with a spin of 0.9, and the radiative efficiency is 0.156. From Figure 12 it is evident that for the rapidly spinning BHs it is much more difficult to become supermassive by

$z = 6$. However, as shown in the right-hand panel of Figure 12, this problem is somewhat alleviated if BH mergers contribute more significantly to the build-up of the SMBH at high redshifts, as is the case when we seed smaller mass haloes with BHs.

It is interesting to ask whether the BH mass growth by accretion in the case of high radiative efficiencies is reduced because a larger fraction of the accreted mass goes into radiation combined with the fact that the Eddington limit is lower, or because the BH thermal feedback is more powerful and tends to shut off the accretion flow. We find that the main reason for the reduced BH growth is the lower Eddington limit in the case of large radiative efficiencies. We therefore conclude that the BHs seeded at $z \sim 12 - 15$, which grow primarily in isolation and are characterized by large radiative efficiencies, *cannot* easily become supermassive by $z = 6$, unless they accrete in a super-Eddington fashion.

Finally, in the left-hand panel of Figure 12 we also show the mass of the most massive BH in the simulated volume evolved with our default BH model, but starting from somewhat larger initial seeds of $10^6 h^{-1} M_{\odot}$ which were placed in all haloes above $10^{10} h^{-1} M_{\odot}$ (magenta star symbols connected with a dashed line). Whereas for $z > 7$ the most massive BH in this run is always more massive than the corresponding BH which grows from a $10^5 h^{-1} M_{\odot}$ seed, at $z \sim 6$ – due to the self-regulated feedback – its final mass is comparable. In fact, its mass evolution is rather similar to the mass evolution of the most massive BH which grows from a $10^5 h^{-1} M_{\odot}$ seed, but has been seeded in a $10^9 h^{-1} M_{\odot}$ halo, as shown in the right-hand panel of Figure 12.

4.7 BH spin evolution due to BH mergers

We have seen in the previous section that BH mergers can contribute to the BH mass assembly, which at least partially alleviates the problem of highly-spinning BHs becoming su-

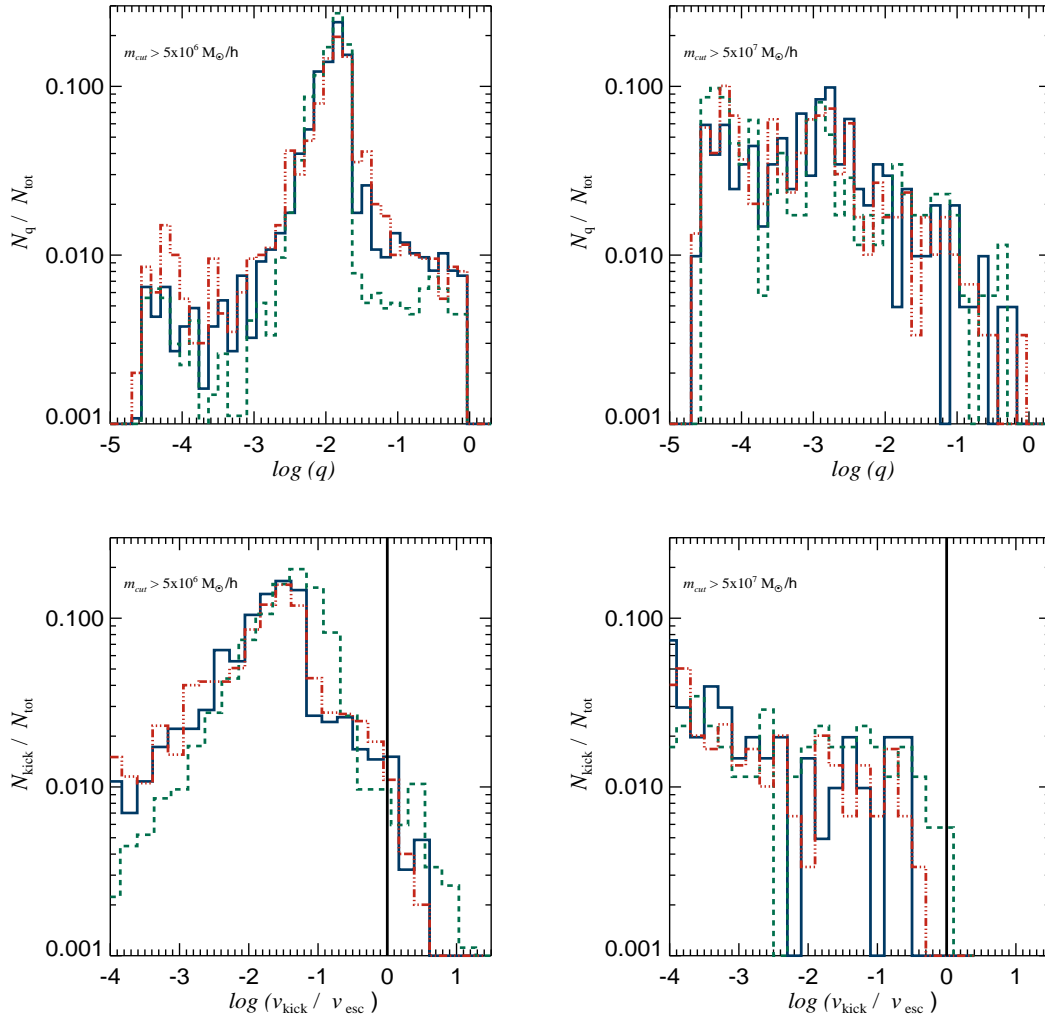


Figure 11. Distribution of mass ratios (upper panels) and kick divided by escape velocities (lower panels) for the same simulations as in Figure 10, using the same colour-coding. However, here the distributions have been computed by considering that at least one of the two merging BHs has to be more massive than $5 \times 10^6 h^{-1} M_{\odot}$ (left-hand panel) and $5 \times 10^7 h^{-1} M_{\odot}$ (right-hand panel), respectively.

permissive. However, BH mergers also modify the spin of the remnant BH and thus could additionally influence the BH mass growth. In order to understand this issue in more depth we have computed the final spin of the remnant BH for every BH merger, taking advantage of the numerical relativity simulations of BH binary mergers (Rezzolla et al., 2008c,b,a). The expected distribution of BH spins at $z = 6$ is illustrated in Figure 13, where we have assumed that the BH spins prior to a merger are parallel (aligned or anti-aligned to the orbital angular momentum with equal probability) and initially characterized by a large spin value of 0.9.

The majority of BHs is spun-down after experiencing several mergers, and hence the resulting BH spin distribution is broad at $z \sim 6$. There is also a small fraction of BHs that are actually spun-up by mergers with other BHs, lying to the right of the vertical dashed line. The peak in the BH spin distribution at $a = 0.9$ mostly comes from BH seeds (or BHs that have accreted very little mass) that have not experienced any merger yet and thus have the initial value of the spin. These BHs are about 15% of the BH popula-

tion at $z = 6$ in our simulated volume. The BHs that are spun-up amount to only 5% of the BH population. They result from mergers where both BH spins are aligned with the orbital angular momentum and both are spinning rapidly if the mass ratio is large (otherwise it is sufficient that the more massive BH has a spin of 0.9). Spin-ups can also occur if the less massive BH has a spin orientation which is anti-aligned, but only in case of small mass ratios. For other orientations, spin-downs are more likely, explaining why our BH spin distribution ends up being biased towards spin values lower than the initial spin (see Hughes & Blandford, 2003, for a detailed discussion).

The above has interesting implications for the BH spin evolution of the massive BHs at high redshift, as illustrated in the inset of Figure 13. Here the cross symbols denote the spin of the most massive BH as a function of redshift. Initially the most massive BH is characterized by a rather large spin value, but then after experiencing several merger events it is spun-down. Thus, its radiative efficiency will get lower as well, allowing it to grow rapidly. However, an im-

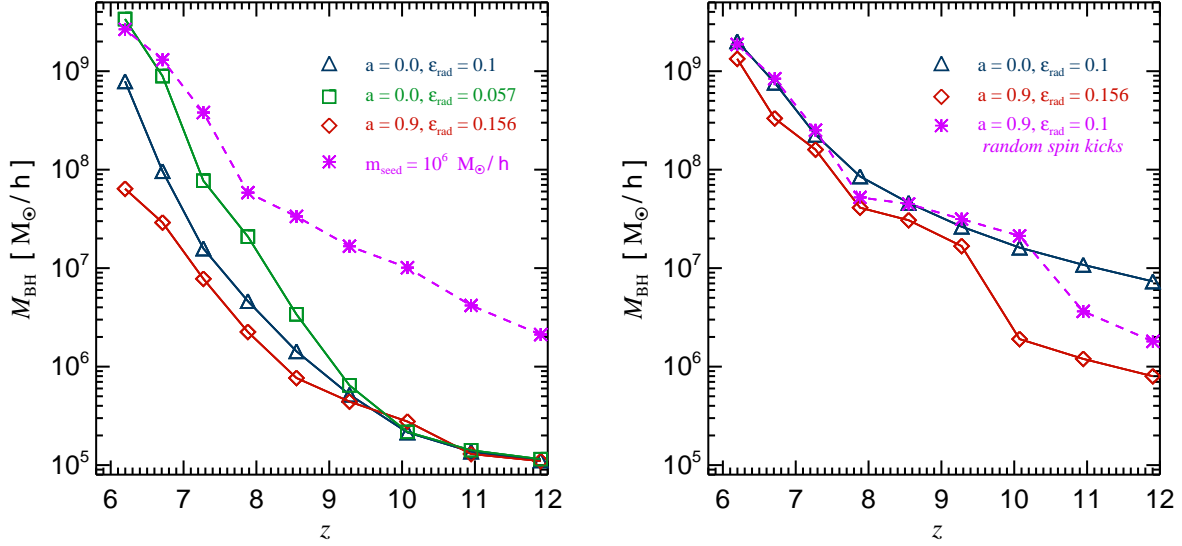


Figure 12. Mass of the most massive BH in the simulated volume as a function of redshift in the runs where BHs are seeded in $\sim 10^{10} h^{-1} M_{\odot}$ haloes (left-hand panel) or in $\sim 10^9 h^{-1} M_{\odot}$ haloes (right-hand panel). Blue triangle symbols denote the BH mass obtained adopting our default model, where BHs are spinless and the radiative efficiency is 0.1. Green square symbols are for a run where BHs are spinless as well, but the adopted radiative efficiency is 0.057 (calculated from equation 8). Red diamond symbols represent the result in the case where all BHs are rapidly spinning, characterized by a spin of 0.9 and a radiative efficiency computed according to equation (8). Finally, magenta star symbols connected with dashed lines in the left-hand panel denote the result of a simulation performed with our default BH model where initial seeds were assumed to be more massive, having $10^6 h^{-1} M_{\odot}$. The magenta symbols in the right panel show the case where gravitational wave recoils with random spin orientations were switched-on.

portant caveat in this conclusion is that in our modelling we have neglected BH spin evolution due to gas accretion itself, which can be expected to certainly play some role. The question then is: Can extended episodes of gas accretion spin up the BH significantly and thus ruin the beneficial effects of BH mergers? Direct numerical simulations of BH accretion flows are needed to give an answer to this interesting question, something we plan to address in our future work.

5 EVOLUTION OF THE FIRST BRIGHT QUASARS FOR $Z < 6$

5.1 Properties of the most massive BH and its host halo down to $z = 2$

Having a numerical model that can successfully reproduce the main properties of high redshift quasars and their hosts it is interesting to study the predictions of this model at lower redshifts. For this, we have used the merger tree of the most massive $z = 6$ Millennium halo and extracted its descendents both at redshifts $z = 4$ and $z = 2$. This gives us suitable target haloes for resimulations that we start again from an initial redshift of $z = 127$. For these runs, we adopt the same BH model, and choose the zoom factors of 5 and 8 (see Table 1 for details). In Figure 14, we show a projected gas density map of the descendent halo at $z = 2.24$. The halo has already become fairly massive, with a virial mass of $\sim 10^{14} h^{-1} M_{\odot}$ (note that at $z = 0$, the descendant is the second most massive galaxy cluster in the whole volume of the Millennium run). With a zoom factor of 5, the halo at $z \sim 2$ has more than 4×10^7 particles within the virial radius

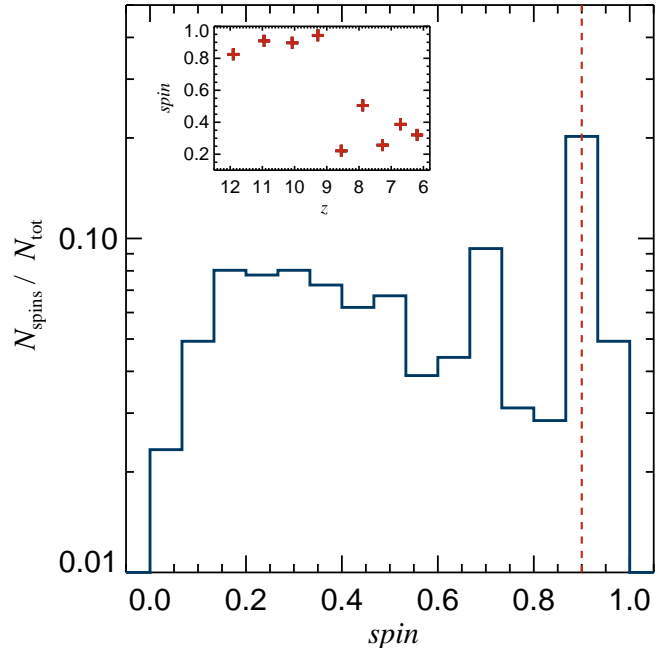


Figure 13. Distribution of BH spins at $z = 6.2$ in the simulation where the initial BH spin is 0.9 and the spins change due to BH mergers. The inset shows the spin of the most massive BH in the simulated volume as a function of redshift.

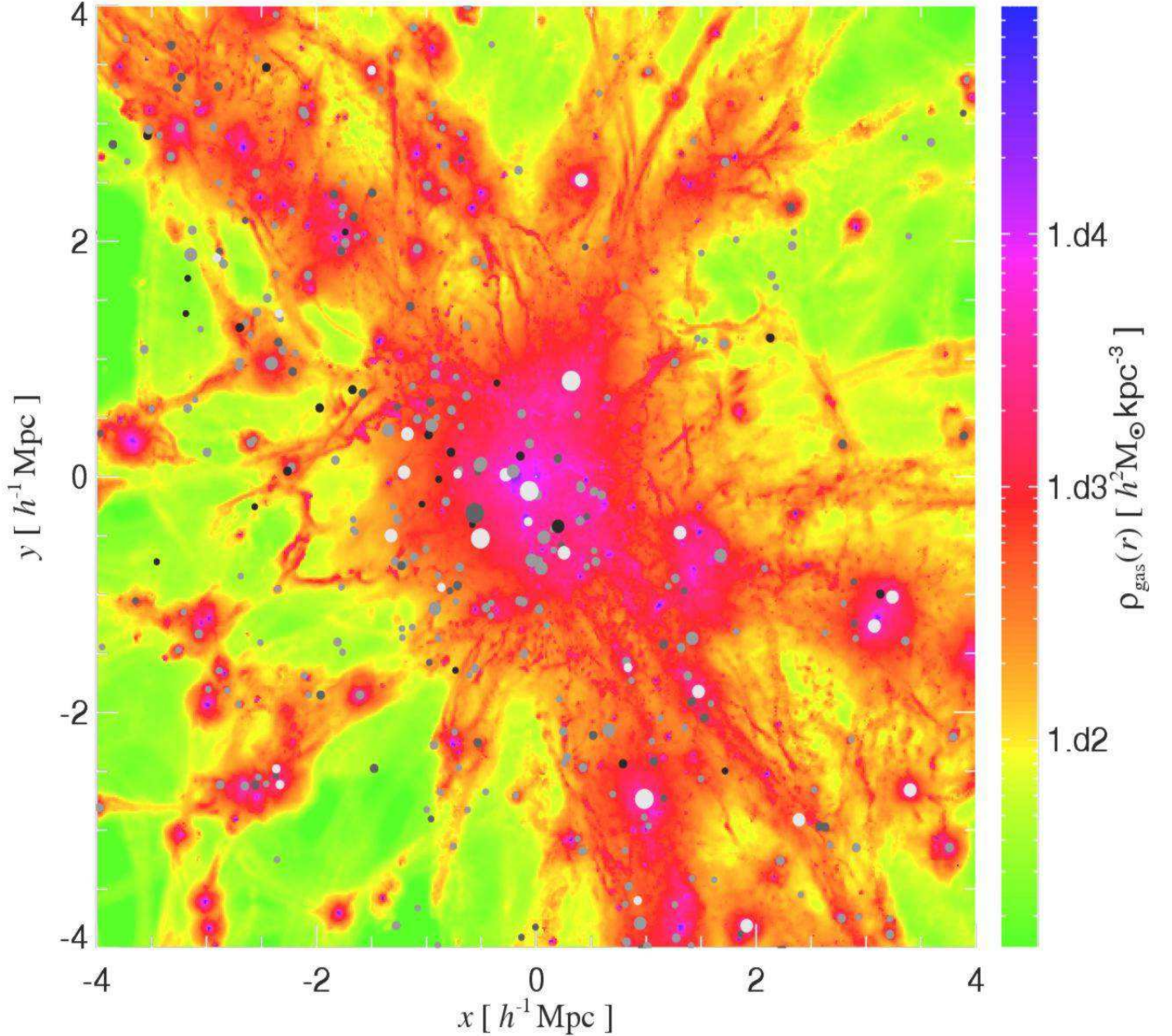


Figure 14. Projected mass-weighted gas density map at $z = 2.24$ of the descendent of the most massive halo at $z = 6$. The halo has reached a mass of $\sim 10^{14} h^{-1} M_{\odot}$, and is connected to a vast number of smaller haloes by an intricate web of filaments. Numerous small scale features and fine details of the ICM and the IGM are visible due to the very large spatial and mass resolution achieved, with more than 10^7 particles within the virial radius of the halo. BHs within the projected slice are shown with coloured dot symbols. The sizes of the dots encode information about the BH mass, with smallest to biggest dots covering the following mass ranges: $10^6 - 10^7 h^{-1} M_{\odot}$, $10^7 - 10^8 h^{-1} M_{\odot}$, $10^8 - 10^9 h^{-1} M_{\odot}$, $> 10^9 h^{-1} M_{\odot}$. The colours of the dots encode the bolometric luminosity of BHs, from black over shades of grey to white, corresponding to the intervals: $< 10^{42} \text{erg s}^{-1}$, $10^{42} - 10^{43} \text{erg s}^{-1}$, $10^{43} - 10^{44} \text{erg s}^{-1}$, and $> 10^{44} \text{erg s}^{-1}$. Note that only two BHs have a bolometric luminosity greater than $10^{45} \text{erg s}^{-1}$, one has a luminosity of $2.2 \times 10^{45} \text{erg s}^{-1}$, and the other $1.1 \times 10^{46} \text{erg s}^{-1}$. The latter is the descendent of our $z = 6$ quasar).

and is embedded within a rich intergalactic environment, with many smaller haloes interconnected by a complex filamentary structure. In Figure 14, the BH particles have been marked with coloured dot symbols. The size of each symbol encodes the BH mass, while the colour-coding reflects the instantaneous bolometric luminosities, where for simplicity we have assumed that all BHs are radiatively efficient with a radiative efficiency of 0.1 (see the figure caption for more details). Besides the central BH, which has the largest mass and the highest bolometric luminosity, a number of other BHs with a range of masses have bolometric luminosities in excess of $10^{43} \text{ erg s}^{-1}$, indicating that their accretion rates are significant. We will come back to this issue later on in this section.

In order to verify that our resimulation technique gives similar results for the BH mass assembly when we extract a descendent of the $z = 6$ halo either at $z = 4$ or at $z = 2$, in Figure 15 we compare the most massive BH in the simulated volume as a function of redshift for both cases. Reassuringly, the BH mass at a given epoch obtained from a resimulation done for the $z = 6$ (blue symbols) halo is very similar to the BH mass obtained from a resimulation done for the $z = 4$ (green diamonds) or $z = 2$ (red squares) most massive descendants. This confirms that these resimulations of the same object extracted at different redshifts give us consistent estimates of the growth of the most massive BH in overlapping redshifts intervals. Furthermore, the green dashed line in Figure 15 shows the BH mass for the resimulations where the host halo has been extracted at $z = 4$ (same as green diamonds), but the numerical resolution was higher, corresponding to a zoom factor of 8 (the other runs considered in the figure have a zoom factor of 5). Given that the mass of the most massive BH in this simulation starts to be indistinguishable for $5 < z < 7$ from the analogous run performed with lower resolution, we are confident that the numerical resolution of 5^3 higher than that of the Millennium simulation is sufficient to resolve the growth of the most massive BH reliably all the way to $z = 2$. Moreover, we have verified that the properties of the host halo (e.g. its mass, gas and stellar content, mean temperature, total SFR) are also recovered very well in all runs performed.

Similarly to the properties of the $z = 6$ halo that are listed in Table 2, the properties of its $z = 4$ and $z = 2$ descendent are summarised in Table 3. From $z \sim 6$ to $z \sim 4$ and from $z \sim 4$ to $z \sim 2$, the BH increases its mass by similar factors of order ~ 3.3 (even though the first redshift interval corresponds to 0.73 Gyr, while the second one is much longer, amounting to 1.6 Gyr), while the BH’s host halo (both in the DM and baryonic components) experiences quite different relative growth, increasing its mass by factors of ~ 4.5 and ~ 7 , respectively. At redshifts higher than 6, the BH increases its mass by a huge factor of $\sim 2 \times 10^4$ from $z \sim 12$ to $z \sim 6$, while the host halo mass grows from $\sim 1.5 \times 10^{10} h^{-1} M_{\odot}$ to $\sim 4.9 \times 10^{12} h^{-1} M_{\odot}$. Therefore, the mass assembly of the host halo and its central BH do not go “hand-in-hand”, and if there is a tight relationship between BH mass and host halo mass (Ferrarese, 2002) it needs to evolve with redshift over the interval considered here (see also e.g. Wyithe & Padmanabhan, 2006; Shankar & Mathur, 2007; Colberg & di Matteo, 2008; Croton, 2009). This also holds true if instead of the host halo dark matter mass we consider the total stellar mass within R_{200} . Finally,

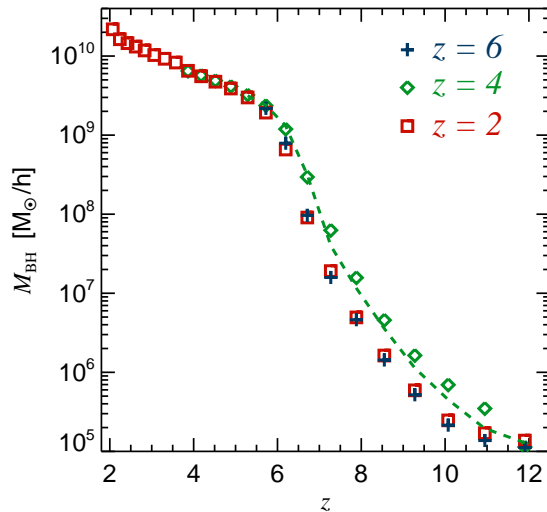


Figure 15. Mass of the most massive BH in the simulated volume as a function of redshift. Blue crosses are for the run where the most massive halo of the Millennium simulation has been selected at $z = 6$ and then was resimulated at 5^3 times better mass resolution. The green diamonds are for the resimulation of the main descendent of our $z = 6$ halo selected at $z = 4$, and resimulated with the same zoom factor of 5. The dashed green line is for the same run but this time performed at even higher resolution adopting a zoom factor of 8. The red squares are for the case where the main descendent of our $z = 6$ halo has been selected at $z = 2$ and was resimulated with a zoom factor of 5. In all runs, the BHs were seeded in haloes with masses larger than $10^{10} h^{-1} M_{\odot}$. The BH mass growth is very similar in all runs performed within the overlapping interval of redshifts and that it does not depend on our choice for the resimulated region.

the fastest growth of the most massive BH at high redshifts, can be viewed as a signature of so-called ‘downsizing’, as we discuss next in more detail.

5.2 The cosmological downsizing of the BH mass accretion

In Figure 16 we examine how efficiently our simulated BHs grow by accretion at different epochs. To this end we show the distribution of BH accretion rates (in $M_{\odot} \text{ yr}^{-1}$) per logarithmic bin of accretion rate in Eddington units at $z = 6.2$ (left-hand panel), $z = 3.86$ (central panel), and $z = 2.07$ (right-hand panel). We both consider the whole population of BHs (black histograms), as well as BHs belonging to specific mass ranges: grey histograms denote the lowest, green hatched histograms the intermediate, and red histograms the highest mass range considered. A number of interesting features can be seen from these plots: (a) for all mass ranges considered, the distribution of Eddington ratios broadens at lower redshifts, implying that the fraction of BH accretion that occurs in the sub-Eddington regime is more significant at later cosmic times; (b) the peak of the BH accretion rate distribution shifts to the left most strongly for the highest mass range considered, indicating that the high-mass end of the BH population experiences faster evolution in the average accretion rate; (c) the same holds true for the interme-

MAIN HALO PROPERTIES AT $z = 3.9$												
Run	N_{200}	$N_{200,DM}$	$N_{200,gas}$	R_{200} [kpc/h]	M_{200} [M_{\odot}/h]	$M_{200,DM}$ [M_{\odot}/h]	$M_{200,gas}$ [M_{\odot}/h]	$M_{200,*}$ [M_{\odot}/h]	T_{200} [K]	SFR [M_{\odot}/yr]	M_{BH} [M_{\odot}/h]	M_{Edd}
with BHs	6240576	2772900	1413716	719.6	2.17×10^{13}	1.87×10^{13}	1.57×10^{12}	1.36×10^{12}	1.2×10^7	1105	6.51×10^9	0.06
MAIN HALO PROPERTIES AT $z = 2.1$												
Run	N_{200}	$N_{200,DM}$	$N_{200,gas}$	R_{200} [kpc/h]	M_{200} [M_{\odot}/h]	$M_{200,DM}$ [M_{\odot}/h]	$M_{200,gas}$ [M_{\odot}/h]	$M_{200,*}$ [M_{\odot}/h]	T_{200} [K]	SFR [M_{\odot}/yr]	M_{BH} [M_{\odot}/h]	M_{Edd}
with BHs	46051219	19457020	12593848	1387.9	1.55×10^{14}	1.31×10^{14}	1.47×10^{13}	9.27×10^{12}	3.7×10^7	2512	2.18×10^{10}	0.01

Table 3. The main properties of the descendants of the most massive Millennium halo at $z = 6$, resimulated to $z = 3.9$ and $z = 2.1$, respectively. BH seeds were introduced in haloes with masses larger than $10^{10} h^{-1} M_{\odot}$, and adopted numerical resolution corresponds to the zoom factor of 5. The second to fourth columns indicate the total, dark matter, and gas particle numbers within the virial radius (fifth column). The total, dark matter, gas, and stellar mass of the halo are listed in columns six to nine. The mean mass-weighted temperature and the total star formation rate within the virial radius are given in columns ten and eleven. The last two columns give the mass of the central BH and the accretion rate in Eddington units.

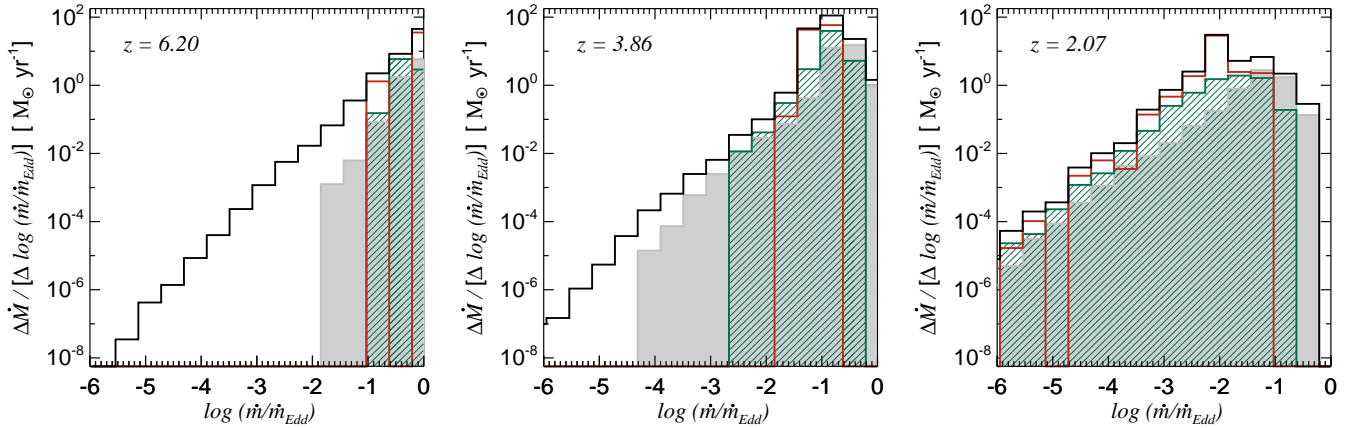


Figure 16. The distribution of BH accretion rate counts (in $M_{\odot} \text{yr}^{-1}$) in logarithmic intervals of BH accretion rate expressed in Eddington units, at three different redshifts as indicated on the panels. The black histogram is for all BHs; The other histograms have been computed taking into account only BHs belonging to a certain mass range: grey histograms are for $10^6 h^{-1} M_{\odot} < M_{BH} \leq 10^7 h^{-1} M_{\odot}$, green hatched histograms are for $10^7 h^{-1} M_{\odot} < M_{BH} \leq 10^8 h^{-1} M_{\odot}$, while the red histograms are for $10^8 h^{-1} M_{\odot} < M_{BH}$. The most massive BHs accrete most efficiently at the highest redshift considered and their BH accretion rate distribution evolves fastest with redshift with respect to the two other mass bins. This can be viewed as a clear signature of “downsizing”.

diate mass range BHs compared with the lowest mass range BHs, thus confirming that there is a systematic trend in the evolution of the peak BH accretion rate with BH mass. All these features are clear signatures of ‘downsizing’ in the BH mass growth, i.e. of a shift of the main activity from high to low masses with cosmic time, running in a opposite sense to the hierarchical build up of cosmic structures (e.g. Barger et al., 2005).

To see this effect in perhaps even clearer way, we plot in Figure 17 the distribution of mean Eddington ratios as a function of BH mass at the same three epochs considered above. For a given BH mass bin, the average Eddington ratio increases with increasing redshift, and the relative increase is most pronounced for the high mass end of the BH mass function.

5.3 Evolution of the intracluster gas properties

We now analyze how the central SMBH affects the properties of the intracluster gas down to low redshift. In Figure 18, we show the change of the gas density, mass-weighted temperature, and gas metallicity (in Solar units) at $z = 7.27$ (blue continuous lines), $z = 3.86$ (green dotted lines), and $z = 2.23$ (red dashed lines). The vertical lines denote the gravitational softening length and the virial radii at these three epochs. While there is some cold dense gas in the innermost regions present at $z = 7.27$, due to the powerful AGN feedback the gas in the central regions is heated at lower redshifts. Furthermore, while the gas metallicity is rather patchy at the highest redshift considered, it becomes much more uniform throughout the hot ICM at later times,

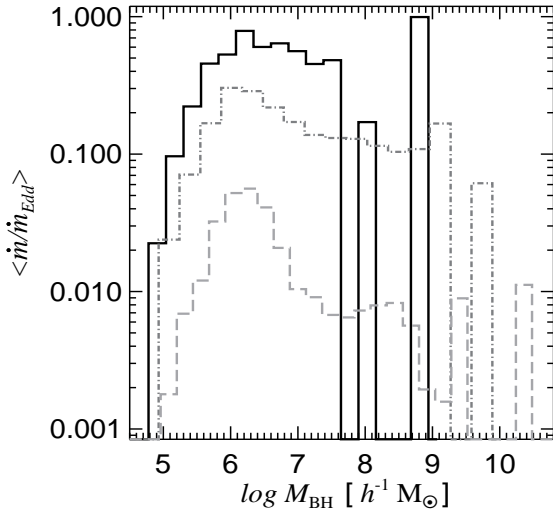


Figure 17. The distribution of the mean BH accretion rates in Eddington units computed per logarithmic BH mass bin at three different redshifts: $z = 6.2$ (black continuous line), $z = 3.86$ (grey dot-dashed line), and $z = 2.07$ (light grey dashed line). For each mass bin the mean BH accretion rate measured in Eddington units increases with increasing redshift, and the relative increase is strongest for the most massive BHs.

which is also caused by AGN feedback. Interestingly, the gas metallicity in the very centre at $z = 7.27$ reaches super-Solar values, after which it declines at $z = 3.86$ to then rise again to super-Solar metallicities at $z = 2.23$. This turns out to be caused by BH feedback as well: highly enriched gas present at early times is transported and mixed by AGN generated outflows with lower metallicity gas further away. Of course, some of the highly enriched gas gets also swallowed by the central BH itself. At later epochs, new generations of stars form in the halo’s central galaxy, and together with metal enriched gas of the infalling satellites, causes the ICM gas metallicity to rise in the central regions again.

5.4 Constraints on the BH growth to $z = 0$ and the presence of ultra-massive BHs

As can be seen from Figure 15 and Table 3, the most massive BH in our simulated volume at $z = 2$ reaches a mass of $\sim 2 \times 10^{10} h^{-1} M_{\odot}$. Several questions immediately arise from this: What causes the BH to become so massive at $z = 2$? What would be its final mass at $z = 0$, and would this be compatible with current observational constraints on the high-mass end of the BH population?

In order to obtain tentative answers to these questions, we have constructed the merger tree of the whole BH population present in our simulated volume and extracted the history of the main progenitor of the most massive BH at $z = 2$. For the BH’s main progenitor, we have also accumulated information about the instantaneous BH mass and accretion rate at each simulation timestep. This data is shown in Figure 19, where we plot the accretion rate in Eddington units (left-hand panel) and the bolometric luminosity (right-hand panel), assuming a constant radiative efficiency of 0.1. After an initial essentially Eddington limited growth,

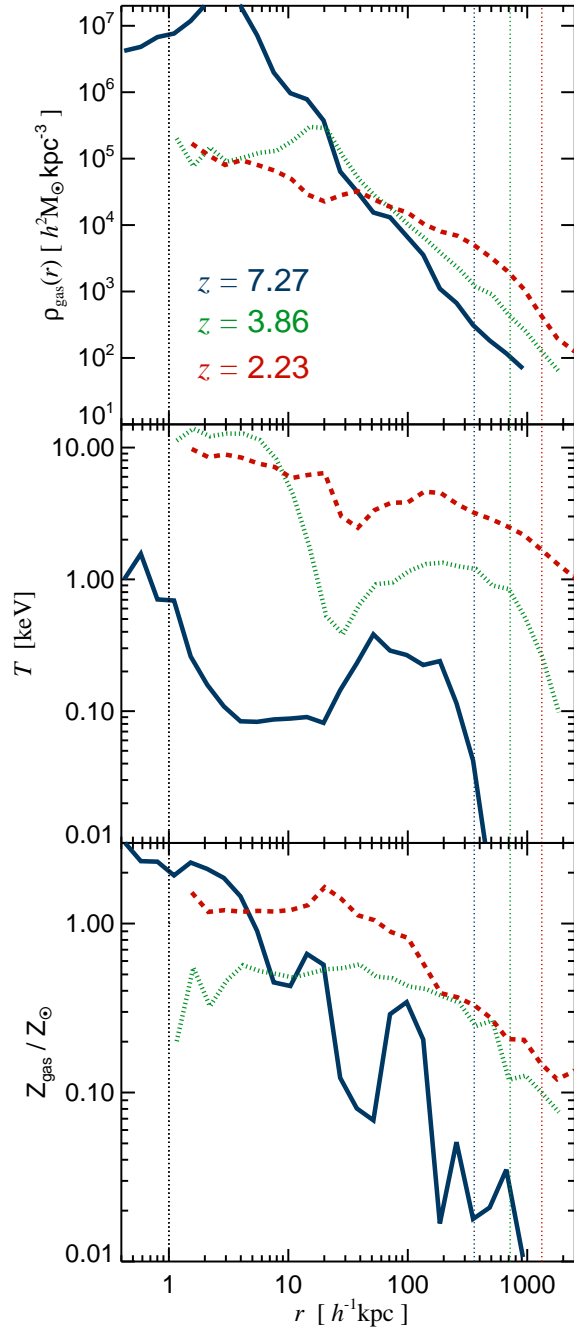


Figure 18. Radial profiles of gas density, mass-weighted temperature and mass-weighted gas metallicity of the resimulated $z = 2$ descendent of the most massive massive halo in the Millennium simulation at $z = 6$, at three different redshifts: $z = 7.27$ (blue continuous lines), $z = 3.86$ (green dotted lines) and $z = 2.23$ (red dashed lines). The simulation has been performed with a zoom factor of 5, and the BHs were seeded in haloes above $10^{10} h^{-1} M_{\odot}$. The vertical dotted lines denote the adopted gravitational softening length and the virial radius of the halo at these three redshifts (in comoving units), using the same colour-coding.

the accretion rate onto the BH's main progenitor is progressively declining for $z < 6$, both in relative and in absolute terms. The red crosses in both panels indicate when the main progenitor undergoes a merger with a massive BH of mass larger than $10^8 h^{-1} M_{\odot}$. The red arrow denotes the time-span during which the host halo of the main BH progenitor experiences a major merger with an almost equal mass halo (the merger mass ratio is 0.8). This shows that there is a relationship between the merging history of the host halo and the activity of the central BH. Note that the peaks in bolometric luminosity do not strictly correspond to the instants of BH mergers, given that the accretion rate is also enhanced by gas which is funnelled towards the central region during halo mergers. This often happens with a time offset relative to the merger event of the BHs.

In Section 5.1, we mentioned that the most massive BH increases its mass by a similar factor of ~ 3.3 over the redshift ranges $z = 6 - 4$ and $z = 4 - 2$. Given that the BH accretion rate is declining with time, this means that the contribution of BH mergers has to be more significant towards lower redshift. In fact, analysis of the merger tree shows that from $z = 6$ to $z = 4$, BH mergers contribute $\sim 20\%$ of the main progenitor mass at $z = 4$, while the BH mergers from $z = 4$ to $z = 2$ contribute up to $\sim 40\%$ of the main progenitor mass at $z = 2$.

We do not have a cosmological simulation at this high resolution all the way to $z = 0$, but we can, nevertheless, try to use our results to estimate a rough upper limit for the mass the most massive BH would attain by the present day. For this, we need to consider contributions both from gas that is locally accreted and also from BHs that are likely to merge with the descendant of the most massive $z = 2$ BH. As for the contribution from accretion, we have fitted a linear relation to the logarithm of the BH accretion rate as a function of cosmic time, and then integrated this result from $t = 3.3$ Gyr to $t = 13.6$ Gyr. This extrapolation yields a total mass of about $\sim 2 \times 10^9 h^{-1} M_{\odot}$ that is expected to be accreted locally by the BH. In order to estimate the contribution to the growth by BH mergers, we have tracked back in time the merger history of the host halo from $z = 0$, based on the Millennium merger trees. We have then assumed that all haloes that merge with our target halo contain a massive BH in their centre, and that all these BHs will merge with our target BH. To estimate the cumulative mass involved in these mergers, we have associated BH masses with dark matter haloes based on the following relation: $M_{\text{BH}}/10^8 M_{\odot} = 0.1(M_{\text{DM}}/10^{12} M_{\odot})^{1.65}$ (Ferrarese, 2002). For the dark matter masses M_{DM} of haloes we have taken the values measured when the haloes were still in separate FoF groups for the last time. With this procedure we conclude that the total mass of all BHs which can potentially merge with the descendant of our $z = 2$ BH is of the order of $\sim 9 \times 10^9 h^{-1} M_{\odot}$ [¶]. Therefore, as an upper limit we are quite confident that our BH will not increase its mass from $z = 2$ to $z = 0$ by more than a factor of 2.

[¶] After undergoing a major merger at $z = 2$ the host cluster has a much more quiet merging history with only one important merger happening at $z = 0.9$, of mass-ratio 0.2. This further justifies our assumption that the BH accretion rate will continue to decrease given that not much fresh gas for accretion can be supplied by merging satellites.

Is a mass of $3 - 4 \times 10^{10} h^{-1} M_{\odot}$ reasonable for the present day descendent of one of the most massive BHs at $z = 6$? Observationally we have no constraints yet on what the duty cycle of the SDSS quasars is, but if the BHs have grown substantially in an Eddington limited accretion regime as in our simulations, the duty cycle has to be close to unity. The local volume for which we can measure BH masses reasonably well is then significantly smaller than that probed by either the SDSS survey or the Millennium simulation. Estimating the mass of the most massive BH expected in such a volume requires therefore a significant extrapolation of the local scaling relations between BH mass and galaxy luminosity (or stellar velocity dispersion) and an estimate of the likewise uncertain space density of rather rare galaxies (see also Natarajan & Treister, 2009).

Recently, an interesting issue regarding a potential mismatch between BH masses estimated from the $M_{\text{BH}} - \sigma$ versus the $M_{\text{BH}} - L$ relation at the high-mass end has been raised by Lauer et al. (2007). Their findings imply that the masses of the most massive BHs are probably underestimated if one uses the $M_{\text{BH}} - \sigma$ relationship, and that at the high mass end of the BH mass function there should be BHs with mass of the order of $\sim 10^{10} M_{\odot}$, which however should be very rare and reside in the most massive galaxy clusters today. Lauer et al. (2007) give an estimate of the cumulative number of BHs above a given mass, which for the mass threshold of $10^{10} M_{\odot}$ yields that there should be only a handful of these ultra-massive BHs in the Millennium simulation volume. This is exactly in line with our findings, which furthermore predict that the most massive BHs today reside in the most massive and very rare haloes, and have powered in their past the most luminous quasars.

However, we caution that one should take our estimate of the mass of the most massive BHs at low redshifts with a grain of salt, in the sense that this is likely to be somewhat at the high end within our model. This is due to several reasons: first, the contribution of BH mergers to the BH mass assembly starts to be more important at lower redshifts, especially for the BH sitting in the centre of the brightest cluster galaxy (see also Ruszkowski & Springel, 2009). Given that our prescription for BH mergers is very efficient (and additionally given that here we have not considered 3-body BH effects and gravitational recoils), our estimate for the contribution of merging BHs to the mass assembly is an upper limit. Additionally, we have not considered that gravitational wave emission carries away part of the rest-mass energy (albeit this effect is probably not very significant), and that non-vanishing BH spins can potentially reduce the amount of material that a hole can accrete (which however could build some tension with the growth of BHs at $z > 6$). Nevertheless, we clearly find that the existence of rare ultra-massive BHs of mass $\sim 1 - 2 \times 10^{10} M_{\odot}$ in our local Universe is a very interesting and plausible possibility. At the same time, this highlights how special most luminous quasars are.

6 DISCUSSION AND CONCLUSIONS

We have studied the growth of BHs at high redshifts with state-of-the-art numerical simulations in the full cosmological context that take into account feedback effects from BH gas accretion. The main objective was to investigate which

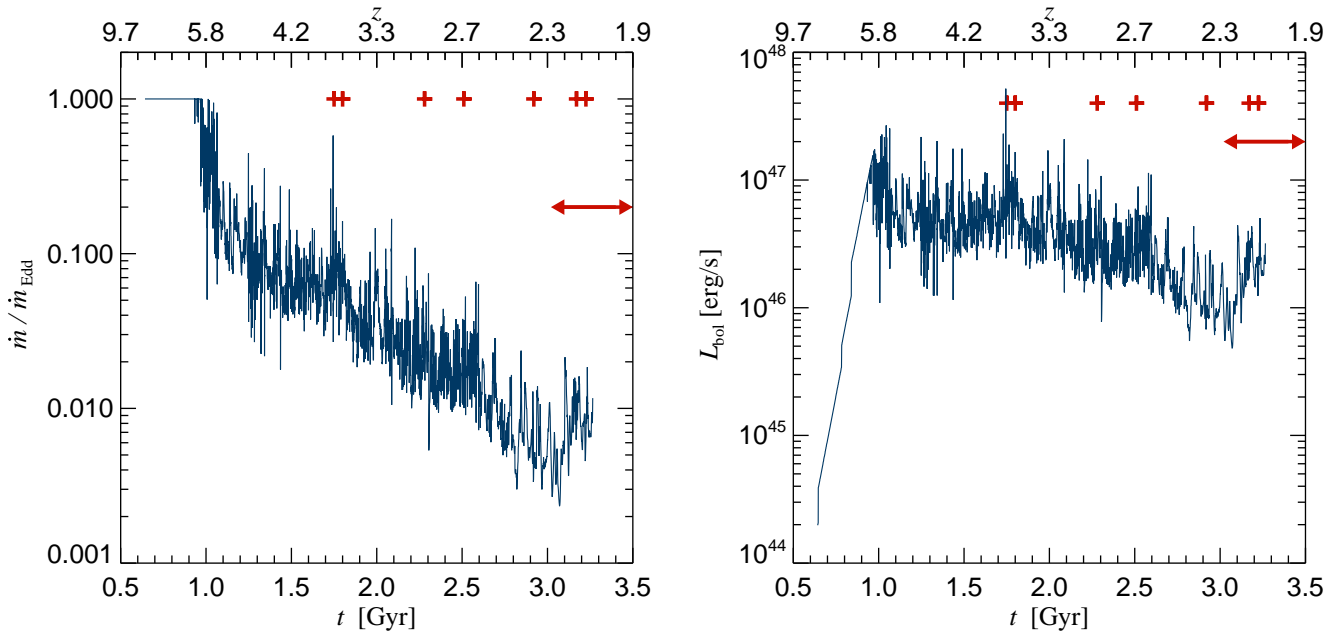


Figure 19. The BH accretion rate in Eddington units (left-hand panel) and the bolometric luminosity (right-hand panel) of the main progenitor of the most massive BH at $z = 2$. At $z < 6$ both quantities start decreasing. The red crosses on both panels indicate mergers of the main progenitor with another BH with mass larger than $10^8 h^{-1} M_{\odot}$. There is a close correspondence between these mergers and the intervals of enhanced accretion. The red arrow denotes the time interval of the most important major merger the host halo undergoes (of mass ratio 0.8), from the redshift where the two FoF haloes first ‘merge’ (or rather touch), to the moment when the surviving core of the secondary halo merges with the core of the primary.

are the most plausible formation scenarios of the SMBHs at $z = 6$ whose existence is inferred from observations of SDSS quasars. For this purpose, we have selected the most massive dark matter halo from the Millennium simulation at $z = 6$, and resimulated it at a much higher mass and spatial resolution, including gas physics, star formation and feedback processes, and a model for BH seeding, growth and feedback. We have first thoroughly tested our model and confirmed that numerical convergence in the SFR and BH accretion rate has been reached. We have then explored the BH growth at high redshift, systematically varying different physical assumptions in the simulations that could potentially help or prevent early BH assembly.

We have found that it is possible in our default BH model to grow SMBHs by $z = 6$ which have a space density, mass, and bolometric luminosity consistent with the findings from the SDSS quasar observations. This is a non-trivial result given that the same model for BH growth and feedback also reproduces the observed BH mass density, the observed relations between BH mass and host galaxy at low redshifts, and alleviates overcooling in massive ellipticals (see Springel et al., 2005b; Sijacki et al., 2007). Regardless of the two different seeding prescriptions we have considered (using halo mass thresholds of $10^9 h^{-1} M_{\odot}$ or $10^{10} h^{-1} M_{\odot}$) the SMBH we form at $z = 6$ gains most of its mass by gas accretion, undergoing extended episodes of Eddington-limited accretion. We have checked whether starburst powered galactic winds can expel a sufficient amount of the central gas supply and thus stall the formation of the SMBH. This is not the case in our simulations. If this mechanism operates in reality, then galactic winds would need to have rather large mass-loading

factors and velocities ($\sim 1000 \text{ km s}^{-1}$), and would have to blow away a substantial fraction of the innermost dense gas which is the reservoir for BH accretion.

We have extended our default model by incorporating prescriptions for gravitational wave induced BH recoils, based on recent numerical relativity simulations of merging BH binaries. We considered both non-spinning and spinning BHs. We have found that a large number of BHs experience gravitational recoils that kick them out of their host haloes (20%-40%, depending on the model adopted). The vast majority of these BHs have low mass, and the probability of expelling more massive BHs is not very high. In our simulations a SMBH still forms even in the presence of strong gravitational wave emission recoils, with very similar mass as in the case without recoils.

However, we would like to point out a potential caveat in our modelling. Since we are primarily interested in how many BHs get kicked out from their hosts, we have only imparted kick velocities to the remnant BHs if the estimated recoil velocity is larger than the escape velocity of the host halo. Otherwise we have neglected the recoil, assuming that the remnant BH stays in the host halo and quickly sinks again to the centre of the halo. This treatment should be adequate as our simulations do not have sufficient resolution to accurately calculate the dynamical friction processes that would bring a displaced BH back to the centre of a halo. Depending on how much material a displaced remnant BH can carry with it and how long it takes the BH to return to the centre, minor recoils could potentially also produce periods of stagnation in the BH mass growth. This is a very

interesting possibility that we have neglected here but plan to investigate in forthcoming work.

The introduction of BH spin in our modelling also allows us to investigate the impact of spin-dependent radiative efficiencies on the BH mass growth. A rapidly spinning BH (with a constant spin of $a \geq 0.9$) seeded at $z \simeq 12 - 15$ will fail to become supermassive by $z = 6$ unless it grows substantially by mergers with other BHs, or can accrete at a super-Eddington rate. On the other hand, if an initially rapidly spinning BH experiences several mergers with other BHs (which are also initially rapidly spinning), and if we compute at each merger the spin of the BH remnant according to the numerical relativity findings, then it appears very likely that the BH will get spun-down and end up with low spin. This suggests that highly spinning BHs which grow in “isolation” (not experiencing many mergers) have the largest difficulty in becoming massive enough by $z = 6$. This conclusion remains valid even when we start from fairly massive BH seeds. We caution however that super-Eddington accretion or the effect of gas accretion on the spin evolution (that we have not considered here) could in principle alleviate this problem.

Finally, we wanted to understand the kinds of objects the first SMBHs in our simulations evolve into, how their properties change with time and whether they are consistent with what we know about the demographics of low redshift BHs. To this end, we have identified the descendants of our $z = 6$ host halo at $z = 4$ and $z = 2$, and resimulated them with the same mass and spatial resolution as before. We have then tracked the accretion rate of the descendent of the most massive BH at $z = 6$ all the way to $z = 2$. The accretion rate becomes systematically more sub-Eddington, and even in absolute terms the accretion rate decreases. At $z \sim 6$ accretion of gas onto the most massive BH changes from Eddington-limited to being limited by the thermal feedback of the AGN implemented in the simulation. Why does this change occur at $z \sim 6$? This can be best understood as a selection effect. The mass of the host haloes necessary to reproduce the space density of SDSS quasars assuming a duty cycle of order of unity and the inferred mass of the BHs are close to the threshold where the AGN feedback in our simulations becomes efficient in shutting off the fuel supply.

Comparing the accretion rates in Eddington units for different mass ranges and at different epochs, we found a clear signature of downsizing of BH accretion rates. While we had seen a hint of this effect in Sijacki et al. (2007), we have here extended and confirmed this finding all the way to very high redshifts, where very rare and massive BHs are accreting efficiently and driving the trend. In this respect, the simulations performed in this study turned out to be ideal to highlight the issue of the downsizing of the BH mass growth by accretion.

At the high resolution achieved here it is too costly to use the same simulation technique down to redshift $z = 0$, but our results up to $z = 2$ can still be used to estimate the mass finally reached at $z = 0$ by the descendant of our most massive BH. We found that the mass should reach a few times $10^{10} h^{-1} M_{\odot}$, taking into account both gas accretion and further BH mergers. This may appear as a rather large mass (and in part is due to the very efficient BH mergers in our model), but note that present observations already

suggest that there should be a handful of ultra-massive BHs with masses of order of $1 - 2 \times 10^{10} h^{-1} M_{\odot}$ in the local Universe. These should be mostly dormant, low activity remnants of the most luminous $z = 6$ quasars which are situated today in the central galaxies of rich galaxy clusters.

It is encouraging that the cosmological simulations examined here provide such a successful simultaneous description of the build-up of SMBHs at high and low redshift, despite the simplicity of our BH growth model that glosses over much of the detailed small-scale physics of accretion flows. It will be very interesting to refine this picture in future with ever more sophisticated cosmological simulations. Among other improvements, this will make it hopefully possible to account more consistently for the origin of the BH seeds, and the spin evolution of BHs due to gas accretion.

ACKNOWLEDGEMENTS

DS acknowledges a Postdoctoral Fellowship from the UK Science and Technology Funding Council (STFC). The simulations were performed on the Cambridge High Performance Computing Cluster DARWIN in Cambridge (<http://www.hpc.cam.ac.uk>).

REFERENCES

- Baker J. G., Boggs W. D., Centrella J., Kelly B. J., McWilliams S. T., Miller M. C., van Meter J. R., 2008, *ApJ*, 682, L29
 Bardeen J. M., Press W. H., Teukolsky S. A., 1972, *ApJ*, 178, 347
 Barger A. J., Cowie L. L., Mushotzky R. F., Yang Y., Wang W.-H., Steffen A. T., Capak P., 2005, *AJ*, 129, 578
 Barth A. J., Martini P., Nelson C. H., Ho L. C., 2003, *ApJ*, 594, L95
 Beckwith K., Hawley J. F., Krolik J. H., 2008, *ApJ*, 678, 1180
 Begelman M. C., Blandford R. D., Rees M. J., 1980, *Nature*, 287, 307
 Begelman M. C., Blandford R. D., Rees M. J., 1984, *Reviews of Modern Physics*, 56, 255
 Begelman M. C., Volonteri M., Rees M. J., 2006, *MNRAS*, 370, 289
 Berti E., Cardoso V., Gonzalez J. A., Spherhake U., Hannam M., Husa S., Brügmann B., 2007, *Phys. Rev. D*, 76, 6, 064034
 Berti E., Volonteri M., 2008, *ApJ*, 684, 822
 Bertoldi F., Carilli C. L., Cox P., Fan X., Strauss M. A., Beelen A., Omont A., Zylka R., 2003, *A&A*, 406, L55
 Bondi H., 1952, *MNRAS*, 112, 195
 Bondi H., Hoyle F., 1944, *MNRAS*, 104, 273
 Bower R. G., Benson A. J., Malbon R., Helly J. C., Frenk C. S., Baugh C. M., Cole S., Lacey C. G., 2006, *MNRAS*, 370, 645
 Bromm V., Loeb A., 2003, *ApJ*, 596, 34
 Campanelli M., Lousto C., Zlochower Y., Merritt D., 2007, *ApJ*, 659, L5
 Campanelli M., Lousto C. O., Zlochower Y., 2008, *Phys. Rev. D*, 77, 10, 101501
 Carilli C. L., et al., 2004, *AJ*, 128, 997
 Ciotti L., Ostriker J. P., 1997, *ApJ*, 487, L105
 Colberg J. M., di Matteo T., 2008, *MNRAS*, 387, 1163
 Croton D. J., 2009, *MNRAS*, 394, 1109
 Croton D. J., et al., 2006, *MNRAS*, 365, 11
 Cuadra J., Armitage P. J., Alexander R. D., Begelman M. C., 2009, *MNRAS*, 393, 1423
 De Villiers J.-P., Hawley J. F., 2003, *ApJ*, 589, 458
 Di Matteo T., Colberg J., Springel V., Hernquist L., Sijacki D., 2008, *ApJ*, 676, 33

- Di Matteo T., Springel V., Hernquist L., 2005, *Nature*, 433, 604
- Dressler A., 1989, in *Active Galactic Nuclei*, edited by D. E. Osterbrock, J. S. Miller, vol. 134 of *IAU Symposium*, 217
- Escala A., Larson R. B., Coppi P. S., Mardones D., 2004, *ApJ*, 607, 765
- Fabian A. C., Iwasawa K., 1999, *MNRAS*, 303, L34
- Fan X., 2006, *New Astronomy Review*, 50, 665
- Fan X., et al., 2001, *AJ*, 122, 2833
- Fan X., et al., 2003, *AJ*, 125, 1649
- Fan X., et al., 2004, *AJ*, 128, 515
- Fan X., et al., 2006, *AJ*, 131, 1203
- Ferrarese L., 2002, *ApJ*, 578, 90
- Ferrarese L., Merritt D., 2000, *ApJ*, 539, L9
- Fitchett M. J., 1983, *MNRAS*, 203, 1049
- Gammie C. F., McKinney J. C., Tóth G., 2003, *ApJ*, 589, 444
- Gao L., White S. D. M., Jenkins A., Frenk C. S., Springel V., 2005, *MNRAS*, 363, 379
- Gebhardt K., et al., 2000, *ApJ*, 539, L13
- González J. A., Spherhake U., Brüggemann B., Hannam M., Husa S., 2007, *Physical Review Letters*, 98, 9, 091101
- Haehnelt M. G., Natarajan P., Rees M. J., 1998, *MNRAS*, 300, 817
- Haehnelt M. G., Rees M. J., 1993, *MNRAS*, 263, 168
- Haiman Z., 2004, *ApJ*, 613, 36
- Häring N., Rix H.-W., 2004, *ApJ*, 604, L89
- Hawley J. F., Krolik J. H., 2006, *ApJ*, 641, 103
- Herrmann F., Hinder I., Shoemaker D., Laguna P., Matzner R. A., 2007, *ApJ*, 661, 430
- Hopkins P. F., Hernquist L., Cox T. J., Di Matteo T., Robertson B., Springel V., 2006, *ApJS*, 163, 1
- Hoyle F., Lyttleton R. A., 1939, in *Proceedings of the Cambridge Philosophical Society*, vol. 35 of *Proceedings of the Cambridge Philosophical Society*, 405
- Hughes S. A., Blandford R. D., 2003, *ApJ*, 585, L101
- Jiang L., et al., 2006, *AJ*, 132, 2127
- Kauffmann G., Haehnelt M., 2000, *MNRAS*, 311, 576
- King A., 2003, *ApJ*, 596, L27
- King A. R., Pringle J. E., 2006, *MNRAS*, 373, L90
- Koide S., Shibata K., Kudoh T., 1999, *ApJ*, 522, 727
- Komatsu E., et al., 2009, *ApJS*, 180, 330
- Koppitz M., Pollney D., Reisswig C., Rezzolla L., Thornburg J., Diener P., Schnetter E., 2007, *Physical Review Letters*, 99, 4, 041102
- Kormendy J., Richstone D., 1995, *ARA&A*, 33, 581
- Kurk J. D., et al., 2007, *ApJ*, 669, 32
- Lauer T. R., et al., 2007, *ApJ*, 662, 808
- Levine R., Gnedin N. Y., Hamilton A. J. S., Kravtsov A. V., 2008, *ApJ*, 678, 154
- Li Y., et al., 2007, *ApJ*, 665, 187
- Lodato G., Natarajan P., 2006, *MNRAS*, 371, 1813
- Lynden-Bell D., 1969, *Nature*, 223, 690
- Magorrian J., et al., 1998, *AJ*, 115, 2285
- Marconi A., Hunt L. K., 2003, *ApJ*, 589, L21
- McKinney J. C., Gammie C. F., 2004, *ApJ*, 611, 977
- Merritt D., Milosavljević M., Favata M., Hughes S. A., Holz D. E., 2004, *ApJ*, 607, L9
- Natarajan P., Treister E., 2009, *MNRAS*, 393, 838
- Okamoto T., Nemmen R. S., Bower R. G., 2008, *MNRAS*, 385, 161
- Pelupessy F. I., Di Matteo T., Ciardi B., 2007, *ApJ*, 665, 107
- Pretorius F., 2007, "Relativistic Objects in Compact Binaries: From Birth to Coalescence", Editor: Colpi et al., Publisher: Springer Verlag, Canopus Publishing Limited, eprint arXiv:0710.1338
- Puchwein E., Sijacki D., Springel V., 2008, *ApJ*, 687, L53
- Rees M. J., 1978, *Phys. Scr*, 17, 193
- Rees M. J., 1984, *ARA&A*, 22, 471
- Regan J. A., Haehnelt M. G., 2009, *MNRAS*, 393, 858
- Rezzolla L., Barausse E., Dorband E. N., Pollney D., Reisswig C., Seiler J., Husa S., 2008a, *Phys. Rev. D*, 78, 4, 044002
- Rezzolla L., Diener P., Dorband E. N., Pollney D., Reisswig C., Schnetter E., Seiler J., 2008b, *ApJ*, 674, L29
- Rezzolla L., Dorband E. N., Reisswig C., Diener P., Pollney D., Schnetter E., Szilágyi B., 2008c, *ApJ*, 679, 1422
- Ruszkowski M., Springel V., 2009, *ApJ*, 696, 1094
- Salpeter E. E., 1964, *ApJ*, 140, 796
- Schmidt M., 1963, *Nature*, 197, 1040
- Shankar F., Croce M., Miralda-Escudé J., Fosalba P., Weinberg D. H., 2008, *ApJ* submitted, eprint arXiv:0810.4919
- Shankar F., Mathur S., 2007, *ApJ*, 660, 1051
- Shapiro S. L., 2005, *ApJ*, 620, 59
- Sijacki D., Pfrommer C., Springel V., Enßlin T. A., 2008, *MNRAS*, 387, 1403
- Sijacki D., Springel V., di Matteo T., Hernquist L., 2007, *MNRAS*, 380, 877
- Silk J., Rees M. J., 1998, *A&A*, 331, L1
- Springel V., 2005, *MNRAS*, 364, 1105
- Springel V., et al., 2005a, *Nature*, 435, 629
- Springel V., Di Matteo T., Hernquist L., 2005b, *MNRAS*, 361, 776
- Springel V., Hernquist L., 2002, *MNRAS*, 333, 649
- Springel V., Hernquist L., 2003, *MNRAS*, 339, 289
- Tanaka T., Haiman Z., 2008, *ApJ* accepted, eprint arXiv:0810.4919
- Thorne K. S., 1974, *ApJ*, 191, 507
- Tremaine S., et al., 2002, *ApJ*, 574, 740
- Umemura M., Loeb A., Turner E. L., 1993, *ApJ*, 419, 459
- Volonteri M., Haardt F., Madau P., 2003, *ApJ*, 582, 559
- Volonteri M., Rees M. J., 2005, *ApJ*, 633, 624
- Volonteri M., Rees M. J., 2006, *ApJ*, 650, 669
- Wang R., et al., 2008, *ApJ*, 687, 848
- Willott C. J., McLure R. J., Jarvis M. J., 2003, *ApJ*, 587, L15
- Wise J. H., Turk M. J., Abel T., 2008, *ApJ*, 682, 745
- Wyithe J. S. B., Loeb A., 2003, *ApJ*, 595, 614
- Wyithe J. S. B., Padmanabhan T., 2006, *MNRAS*, 366, 1029